Journal of Manufacturing Processes 79 (2022) 827–843

Contents lists available at ScienceDirect

Journal of Manufacturing Processes

journal homepage: www.elsevier.com/locate/manpro

Non-isometric dual-spline interpolation for five-axis machine tools by FIR filtering-based feedrate scheduling using pseudo curvature under axial drive constraint

De-Ning Song [a,*], De-Wei Zheng [b], Yu-Guang Zhong [a], Jian-Wei Ma [c], Jing-Song Li [a]

[a] College of Mechanical and Electrical Engineering, Harbin Engineering University, Harbin 150001, China
[b] College of Aerospace and Civil Engineering, Harbin Engineering University, Harbin 150001, China
[c] Key Laboratory for Precision and Non-traditional Machining Technology of the Ministry of Education, School of Mechanical Engineering, Dalian University of Technology, Dalian 116024, China

ARTICLE INFO

Keywords:
Non-isometric dual-spline toolpath
Five-axis interpolation
Feedrate scheduling
FIR filtering
Pseudo curve

ABSTRACT

Due to the nonlinear relationship between workpiece-space and joint-space motions of five-axis machine tools, feedrate scheduling for dual-spline interpolation is acknowledged as a challenging task. Existing methods mainly employ iterative computation, repetitive toolpath discretization, or large feedrate margin, to solve the nonlinear problem. To avoid them, this paper presents a FIR (finite-impulse-response) filtering-based dual-spline interpolation algorithm using pseudo curves. A 3D translational-axis pseudo curve and a 2D rotary-axis pseudo curve are proposed as intermediaries to reduce the dimension of five-axis feedrate-scheduling problem thus figuring out partial nonlinear matters. The FIR filtering is employed to smooth the low-order continuous or even discontinuous axis velocities, to the jerk bounded ones, which further tackles the rest of the nonlinear matters. Although above methods solve the nonlinear issue, they induce new problems which are defined as the filtering-induced-tooltip-contour-error (FITCE) and the filtering-induced-tool-orientation-contour-error (FIOCE) here. To deal with these new problems, two extra constraints, namely the FITCE/FIOCE limitation and a frequency limitation, are added into the interpolation process beyond routine axis drive limitations. Additionally, the presented method does not require constant distance between two splines of the toolpath, which indicates that it is suitable for non-isometric dual-spline toolpath as well. Illustration and experimental tests demonstrate that the presented method merely conducts one-step toolpath discretization without iteration, and performs well in both motion efficiency and smoothness, as well as in real-time capability.

1. Introduction

Five-axis CNC (computer-numerical-control) machine tools are of great importance in machining of complex surfaces and structures such as marine propellers and turbine blades [1,2]. Performances of the interpolation algorithm in the CNC systems play key roles for the machining quality and productivity of the machine tools [3,4]. Currently, the dual-spline interpolator of five-axis machine tools has received increasingly higher attention due to its probability of realizing high speed and high smoothness machining [5,6]. However, scheduling of the feedrate of the dual-spline toolpath remains a challenging task and is always acknowledged as a fundamental problem that should be solved or optimized in multi-axis motion/machining fields [6,7].

The challenging of the dual-spline toolpath feedrate scheduling is originated from the nonlinear relationship between the workpiece space coordinates and the joint space coordinates of machine tools [7]. The feedrate in workpiece space should be planned as high as possible under the smoothness and axial drive constraints in the joint space, overcoming the difficulties caused by the nonlinear matters [8,9]. Existing feedrate scheduling methods for dual-spline interpolation or other kinds of multi-axis motion can mainly be classified into three categories: (1) the convex optimization method, (2) the iterative adjustment method, and (3) the bi-direction scanning-based method.

The convex optimization method aims at transforming the feedrate scheduling into a convex optimization problem and then finding its numerical solution, thus obtaining the optimal feedrate profile. Representative eminent publications of this category are introduced as follows. Dong et al. [10] established a minimum-time trajectory

* Corresponding author.
E-mail address: songdening@hrbeu.edu.cn (D.-N. Song).

https://doi.org/10.1016/j.jmapro.2022.05.023
Received 1 January 2022; Received in revised form 7 May 2022; Accepted 9 May 2022
Available online 25 May 2022
1526-6125/© 2022 The Society of Manufacturing Engineers. Published by Elsevier Ltd. All rights reserved.

optimization model with the constraints of geometric chord error and the axial velocity, acceleration, and jerk, then, the phase plane was utilized for solving of the optimization model. Debrouwere et al. [11] solved the time-optimal path tracking problem under velocity and acceleration constraints by applying a sequence convex scheduling method. Erkorkmaz et al. [12] introduced a pseudo jerk which was computed as the square of the jerk for establishing the optimization model, and solved it by simple linear scheduling method. The linear scheduling approach had also been used by Sun et al. [13] for generating five-axis feedrate with both machine drive and process limits. To release the real-time computational burden, the optimization model was solved in a piecewise linear scheduling manner. Lu et al. [14] transformed the feedrate scheduling to a time-optimal problem through simplifying the constraints in joint space and those for the cutting tool, and it was then solved by numerical integration. Sang et al. [15] obtained the constrained feedrate profile under nonlinear geometric error and axis kinematics limitations, and smoothed the final feedrate through combination of morphological filtering and S-shape acceleration/deceleration mode.

The iterative adjustment method takes a spline with multiple control points to represent the feedrate profile of a corresponding toolpath, then, iteratively adjusts the feedrate spline as high as possible without exceeding the considered constraints. The representative eminent iterative adjustment methods are introduced as follows. Sencer et al. [16] expressed the feedrate profile via a B spline, and the final feedrate profile with programed feedrate and axis drive constraints was obtained by adjusting the B-spline control points iteratively. Beudaert et al. [17] discretized the five-axis toolpath with an equal time step and scheduled drive constrained feedrate using the dichotomy method. Sun et al. [18,19] presented a curve evolution-based feedrate profile scheduling method by their proposed easy-to-implement proportional adjustment algorithm. Liang et al. [20] scheduled the near time-optimal B-spline feedrate profile by rising the control points of it iteratively under jerk constraints. Later, Liang et al. [21] further proposed a global time-optimal feedrate scheduling method through progressive knot insertion and genetic-algorithm-based optimization that are used to determine the knot vector and control points of the B-spline feedrate profile.

The bi-direction scanning-based method first discretizes the toolpath into points, then, scans them and checks the maximum allowable feedrate under multiple constraints in a backward manner to determine the deceleration points, and after that, scans and checks in a forward manner to determine the acceleration points. The representative eminent bi-direction scanning-based methods are introduced as follows. Ma et al. [7] classified the discretized points of the dual-NURBS toolpath into feedrate-sensitive regions and non-sensitive regions, and scheduled the regional feedrate values including acceleration/deceleration-start points by bi-direction scanning. Song et al. [22] improved its motion efficiency afterwards by further subdividing the toolpath into three categories of regions in terms of full-sensitive, semi-sensitive, and non-sensitive regions. Li et al. [23] proposed a novel five-axis feedrate scheduling method with surface characteristic constraints based on quintic feedrate profile, and the minimum-time acceleration/deceleration procedures were also planned by bi-direction scanning. Song et al. [24] proposed an interval-adaptive feedrate scheduling method for long five-axis dual-spline toolpath, in which the discretizing and scanning were employed interval by interval so as to save the real-time computation burden.

Based on above analyzation of three categories of existing feedrate scheduling methods, it can be concluded that most of them require beforehand discretizing of the toolpath or iterative computations. However, during the toolpath discretizing, a shorter discretizing step yields higher precision but heavier computation burden, and vice versa, therefore, it is hard to determine a best discretizing step because it varies with different toolpath geometries. In addition, the iterative computation-based methods can hardly be used in real-time due to the unfixed processing time length. Beyond those, it can also be seen that most existing methods were presented for the isometric dual spline toolpath. However, the generation of strict isometric splines in post processing is a difficult task [6,25,26].

To deal with above mentioned problems, this paper presents a non-isometric dual spline interpolation algorithm for five-axis machine tools by Finite Impulse Responding (FIR) filtering-based feedrate scheduling. The presented method does not require any repetitive spare toolpath discretizing or iterative computations. The whole algorithm is derived without using a fixed distance between the two spline curves of the toolpath, which means that the method is suitable for non-isometric dual spline toolpath. Note that although there exists FIR filtering-based feedrate scheduling and interpolation methods in literatures [27–32], the proposed one is intrinsically different to them, and the differences are analyzed as follows.

First, with respect to the three-axis interpolation, the FIR filtering-based interpolation methods proposed by Tajima et al. [27] and Hayasaka et al. [28] established the relationships between the transformation angle, the feedrate value, and the cornering error for linear and circular toolpaths, i.e., G01 and G02/G03 moves, so that a light-weight corner smoothing can be realized under a tolerance constraint without spline fitting-based geometric smoothing. Additionally, Song et al. [29] proposed a FIR filtering-based real-time interpolation method for pure spline toolpaths, and later they improved their method for the real-time global smoothing of short-line-segment toolpaths [30]. Different to above methods which performs well in three-axis interpolation, the proposed FIR filtering-based method aims at five-axis interpolation, in which not only three translation axes but also two rotary axes should be considered synchronously, which induces nonlinear relationship between the workpiece space and the joint space.

Second, with respect to the five-axis interpolation, Liu et al. [31] established a scaling principle to synchronize the translational and rotary motions with respect to the time durations of the FIR filters, and proposed a FIR filtering-based interpolation method for linear toolpath, i.e., G01 moves, by one-step overlapping of the adjacent toolpath-filtering-signal profiles under corner error and jerk constraints. The method has excellent performances on both interpolation precision and motion smoothness. In addition, Tajima et al. [32] considered path blending errors in Cartesian (Euclidian) as well as in spherical (orientation) coordinates for five-axis G01 linear toolpaths, and realized the non-stop five-axis local smoothing interpolation in real time by matching time-constants of FIR filters utilized for translational and rotational interpolation. This method performs well in computational efficiency, which makes it suitable for real-time application. Comparing with above methods which have excellent performances on G01 linear toolpaths, the proposed FIR filtering-based interpolation method aims at the interpolation of five-axis dual-spline toolpaths whose curvature varies freely and frequently, which is different to the interpolation of linear toolpaths whose curvature is always zero.

To sum up, when comparing with existing FIR filtering-based methods which have advantages for interpolation of three-axis toolpaths and five-axis linear toolpaths, the proposed method mainly suits the interpolation of five-axis dual-spline toolpaths specifically; additionally, when comparing with existing five-axis spline interpolation methods, the proposed method has advantages for real-time applicability because it works without either extra toolpath discretizing or iterative computation. The following sections are organized as follows. The basic idea and detail procedures of the proposed method are presented in Section 2. Illustration and experimental results are discussed in Section 3, and Section 4 summarized the whole paper.

2. General idea and detail procedures of the proposed method

This section first introduces the basic idea of the proposed five-axis dual-spline feedrate scheduling and interpolation method in Section 2.1, including the basic theories that will be used, then, the detail procedures are derived in Section 2.2.

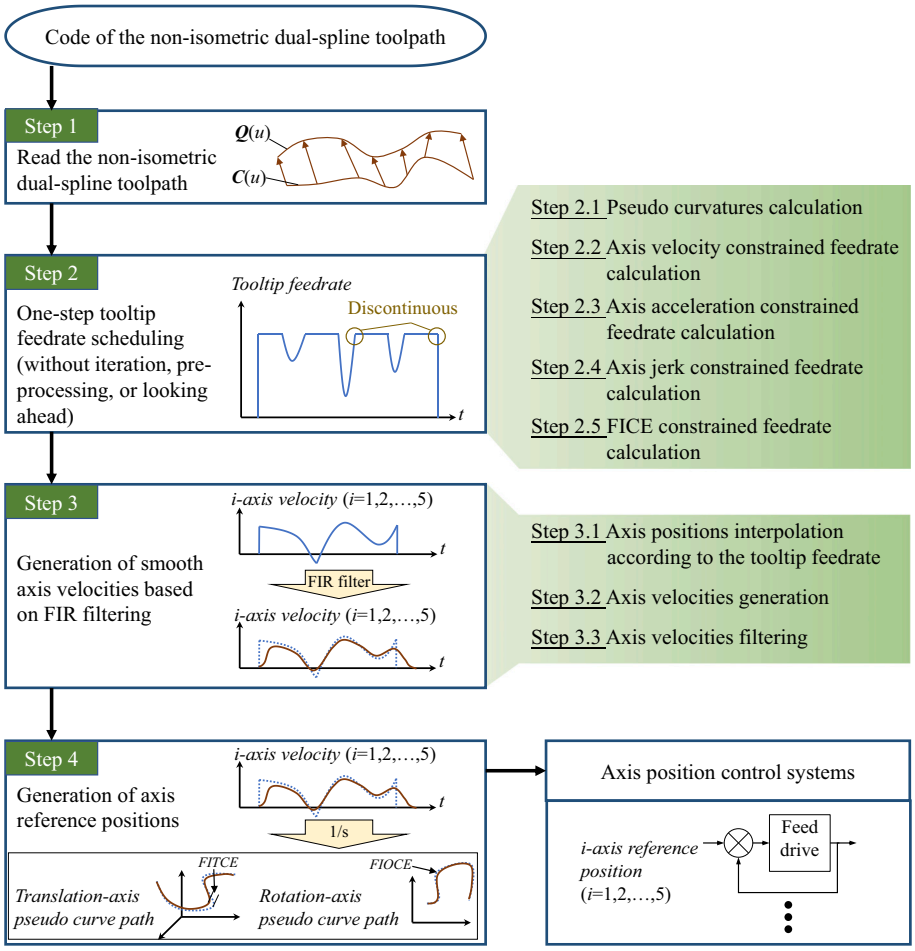

Fig. 1. Overall outline of the presented five-axis interpolation method.

2.1. General idea of the proposed method

Denote $\boldsymbol{q} \in \mathbb{R}^5$ as the five-dimensional axis position vector, and additionally, denote $v_{tip} \in \mathbb{R}^+$ and $\boldsymbol{v}_{axis} \in \mathbb{R}^5$ as the velocities of work-piece space tooltip and joint-space feed axes, respectively. Correspondingly, denote $a_{tip} \in \mathbb{R}^1$ and $\boldsymbol{a}_{axis} \in \mathbb{R}^5$ as tooltip and feed-axis accelerations, respectively, and denote $j_{tip} \in \mathbb{R}^1$ and $\boldsymbol{j}_{axis} \in \mathbb{R}^5$ as tooltip and feed-axis jerks, respectively. Thus, the relationship between tooltip motion and joint axes motion kinematics can be derived as

$$\begin{cases} \boldsymbol{v}_{axis} = \dfrac{d\boldsymbol{q}}{dt} = \dfrac{d\boldsymbol{q}}{ds} \bullet \dfrac{ds}{dt} = \boldsymbol{q}_s v_{tip} \\ \boldsymbol{a}_{axis} = \dfrac{d\boldsymbol{v}_{axis}}{dt} = \dfrac{d\left(\boldsymbol{q}_s v_{tip}\right)}{dt} = \dfrac{d\boldsymbol{q}_s}{ds}\dfrac{ds}{dt} v_{tip} + \boldsymbol{q}_s \dfrac{dv_{tip}}{dt} = \boldsymbol{q}_{ss} v_{tip}^2 + \boldsymbol{q}_s a_{tip} \\ \boldsymbol{j}_{axis} = \dfrac{d\boldsymbol{a}_{axis}}{dt} = \dfrac{d\left(\boldsymbol{q}_{ss} v_{tip}^2 + \boldsymbol{q}_s a_{tip}\right)}{dt} = \dfrac{d\boldsymbol{q}_{ss}}{dt} v_{tip}^2 + \boldsymbol{q}_{ss} \dfrac{dv_{tip}^2}{dt} + \dfrac{d\boldsymbol{q}_s}{dt} a_{tip} + \boldsymbol{q}_s \dfrac{da_{tip}}{dt} \\ = \dfrac{d\boldsymbol{q}_{ss}}{ds}\dfrac{ds}{dt} v_{tip}^2 + 2\boldsymbol{q}_{ss} v_{tip} \dfrac{dv_{tip}}{dt} + \dfrac{d\boldsymbol{q}_s}{ds}\dfrac{ds}{dt} a_{tip} + \boldsymbol{q}_s j_{tip} = \boldsymbol{q}_{sss} v_{tip}^3 + 3\boldsymbol{q}_{ss} v_{tip} a_{tip} + \boldsymbol{q}_s j_{tip} \end{cases} \tag{1}$$

Above, s represents the tool-tip spline arc length parameter, and $\boldsymbol{q}_s$ represents the derivative of $\boldsymbol{q}$ with respect to s. It can be seen from Eq. (1) that merely the relationship between axis velocity $\boldsymbol{v}_{axis}$ and tooltip velocity v_{tip} is linear, and the relations in acceleration and jerk levels are all inherently nonlinear and coupled. The axial acceleration is affected by not only the tooltip acceleration, but also the tooltip velocity. The axial jerk is affected by not only the tooltip jerk, but also the tooltip velocity and acceleration. Therefore, either iterative computations or large margins should be taken for decoupling the relations when scheduling the tooltip feedrate using Eq. (1). This is why most existing methods requires pre-processing or iterations.

To solve above problem, this study merely uses the first formula which is linear in Eq. (1) to schedule the feedrate constrained by axial velocities, and the feedrate values constrained by axial accelerations and axial jerks are further obtained by employing pseudo curvatures in the joint space, thus avoiding to use the second and third formula which are nonlinear in Eq. (1).

The physical meaning of the pseudo curves mentioned in this study and its difference with normal curves are introduced below. As is widely acknowledged, the normal toolpath curves are defined in Cartesian frame, and they represent the motion paths of the tooltip and the tool orientation. The pseudo curves mentioned in this paper are defined in machine-tool joint space, and they represent the motion paths of the virtual particle driven by three translational axes and the virtual particle driven by two rotary axes. The coordinates of the pseudo curves here are virtually defined by joint axes. In addition, the equations and geometries of the pseudo curves are not used here, but only the geometric curvatures of the pseudo curves are derived and utilized in this paper. By doing this, the dimension of the feedrate-scheduling problem can be reduced so as to release the effects of nonlinearity, via the implement of the pseudo curves as intermediates. Details are introduced below.

During five-axis machining, the synergetic motions of five feed axes result in the desired tooltip and tool-orientation motions. The five feed axes contain three translational axes and two rotational axes. What matters for machining quality in reality is the path of tool motion instead of the axes motion. Even though, this study regards the 3D motion path formed by three translational axes and the 2D motion path formed by

two rotational axes as two virtual pseudo curves, and the curvatures of them are named here as pseudo curvatures of translational path and rotational path, respectively. Thus, schedule the pseudo feedrate values of the translational and rotational paths under axial acceleration and axial jerk constraints based on the pseudo curvatures becomes an integration of a 3D scheduling and a 2D scheduling problems, which reduces the dimension of the 5D five-axis feedrate scheduling problem. After that, the scheduled feedrate values of two pseudo curves can be transformed to the tooltip feedrate.

Although the intervene of two pseudo curves reduces the dimension of the five-axis feedrate scheduling problem, the variation of feedrate also affects the axis acceleration and jerk values. To make sure the axis kinematics can be limited in one-step scheduling without iteration, this study sees the axis velocities as time-domain signals, and filters them by a chain of two Finite Impulse Response (FIR) filters. The models of the FIR filter in time domain and Laplace domain are

$$m(t) = \frac{1(t) - 1(t-T)}{T}, 1(t) = \begin{cases} 1, t \geq 0 \\ 0, t < 0 \end{cases} \tag{2}$$

and

$$M(s) = \frac{1 - e^{-Ts}}{Ts} \tag{3}$$

respectively, where T stands for the delay time constant. It has been demonstrated by our previous study [29,30] that after the filtering of two cascaded FIR filters, C^1 continuity of the feedrate profile can be realized thus the jerk can be limited, even though the original feedrate profile before filtering is discontinuous. Therefore, it is not necessary to take the continuity of the feedrate into consideration when scheduling the feedrate before filtering, which dispenses with the need for iterative calculations.

It should be noted that although the FIR filtering-based scheduling releases the iteration, it will inevitably induce contour errors during path tracking, since the filtering improves the continuity of the toolpath, which must alter the path geometry more or less. This error is defined as Filtering Induced Contour Error (FICE) in our previous studies [29,30], and has been constrained by establishing the relation between it and the feedrate. However, in this study, the FICEs of the translational-axis pseudo curve and of the rotational-axis pseudo curve have coupling effects on the workpiece space tooltip contour error and tool-orientation error, which makes the feedrate scheduling under the FICE constraint a new problem. This study further models the relation between the feedrate value and the Filtering Induced Tool-Tip Contour Error (FITCE) and Filtering Induced Tool-Orientation Contour Error (FIOCE), thus obtaining the five-axis FICE constrained feedrate.

Based on above analyzation, the integral procedure of the proposed five-axis interpolation method is outlined as follows and is also shown in Fig. 1.

Step 1. Read the code of the non-isometric dual-spline toolpath, thus obtaining the tooltip motion spline $\boldsymbol{C}(u)$ which represents the motion path of the tooltip, and the tool-axis point motion spline $\boldsymbol{Q}(u)$ which represents the motion path of a point on the tool axis beyond the tooltip.

Step 2. Scheduling the tooltip feedrate in one step, which does not require any iterations, pre-processing, or looking ahead. In this step, there are five sub steps. First, calculate the geometric information of the pseudo curves such as the pseudo curvatures according to $\boldsymbol{C}(u)$ and $\boldsymbol{Q}(u)$. After that, calculate the axis velocities constrained feedrate, the axis accelerations constrained feedrate, the axis jerks constrained feedrate, and the FITCE and FIOCE constrained feedrate.

Step 3. Generation of the smooth axis velocities. In this step, the axis positions are first generated according to the feedrate scheduled in Step 2. After that, the axis velocities are obtained by differentiating the axis positions. Finally, filter the axis velocities by two cascaded FIR filters, so that the smoothness and axis accelerations and jerks can be ensured.

Step 4. Integral of the smoothed axis velocities thus obtaining the axis positions. The axis positions generated in this step are input to the axis position control systems, which completes the function of five-axis interpolation. Note that there exists FITCE and FIOCE between the paths generated in this step and the desired paths, but the errors can be constrained by the scheduled feedrate in Step 2.

Details of above steps are further presented in the following section.

2.2. Detail of the proposed method

In this section, details of main steps of the proposed five-axis interpolation method are derived, in which it can be seen that the computations in all processes are convenient and efficient.

2.2.1. Generation of pseudo-curve geometries

This paper sees the virtual paths by three translational axes and by two rotary axes of the five-axis machine tools as two pseudo curves, so that the dimension of the feedrate scheduling problem can be reduced. Geometries of the pseudo curves are computed as follows, according to the information of the dual spline toolpath.

First, the tangential vector $\boldsymbol{T}_{tip}$, normal vector $\boldsymbol{N}_{tip}$, and binormal vector $\boldsymbol{B}_{tip}$ of the tool-tip motion can be obtained using the tool-tip curve $\boldsymbol{C}(u)$ as

$$\begin{cases} \boldsymbol{T}_{tip}(u) = \dfrac{\boldsymbol{C}'(u)}{\|\boldsymbol{C}'(u)\|} \\ \boldsymbol{B}_{tip}(u) = \dfrac{\boldsymbol{C}'(u) \times \boldsymbol{C}''(u)}{\|\boldsymbol{C}'(u) \times \boldsymbol{C}''(u)\|} \\ \boldsymbol{N}_{tip}(u) = \dfrac{\boldsymbol{C}'(u) \times \boldsymbol{C}''(u) \times \boldsymbol{C}'(u)}{\|\boldsymbol{C}'(u) \times \boldsymbol{C}''(u) \times \boldsymbol{C}'(u)\|} \end{cases} \tag{4}$$

Above, $\boldsymbol{C}'(u)$ means the derivative of $\boldsymbol{C}$ with respect to the parameter u. Since the distance between the tool-tip curve and tool-axis curve is non-isometric, the unit tool-orientation vector $\boldsymbol{Or}$ can be computed as

$$\boldsymbol{Or}(u) = \frac{\boldsymbol{Q}(u) - \boldsymbol{C}(u)}{\|\boldsymbol{Q}(u) - \boldsymbol{C}(u)\|} \tag{5}$$

Hence, the first and second order derivative vectors of the tool-orientation motion can be derived as

$$\begin{cases} \boldsymbol{Or}'(u) = \dfrac{\boldsymbol{Q}'(u) - \boldsymbol{C}'(u)}{\|\boldsymbol{Q}(u) - \boldsymbol{C}(u)\|} - \dfrac{(\boldsymbol{Q}(u) - \boldsymbol{C}(u))^T(\boldsymbol{Q}'(u) - \boldsymbol{C}'(u))}{\|\boldsymbol{Q}(u) - \boldsymbol{C}(u)\|^3}(\boldsymbol{Q}(u) - \boldsymbol{C}(u)) \\ \boldsymbol{Or}''(u) = \dfrac{\boldsymbol{Q}''(u) - \boldsymbol{C}''(u)}{\|\boldsymbol{Q}(u) - \boldsymbol{C}(u)\|} - \dfrac{2(\boldsymbol{Q}(u) - \boldsymbol{C}(u))^T(\boldsymbol{Q}'(u) - \boldsymbol{C}'(u))}{\|\boldsymbol{Q}(u) - \boldsymbol{C}(u)\|^3}(\boldsymbol{Q}'(u) - \boldsymbol{C}'(u)) \\ -\left[\dfrac{\|\boldsymbol{Q}'(u) - \boldsymbol{C}'(u)\|^2 + (\boldsymbol{Q}(u) - \boldsymbol{C}(u))^T(\boldsymbol{Q}''(u) - \boldsymbol{C}''(u))}{\|\boldsymbol{Q}(u) - \boldsymbol{C}(u)\|^3} - \dfrac{3\left((\boldsymbol{Q}(u) - \boldsymbol{C}(u))^T(\boldsymbol{Q}'(u) - \boldsymbol{C}'(u))\right)^2}{\|\boldsymbol{Q}(u) - \boldsymbol{C}(u)\|^5}\right](\boldsymbol{Q}(u) - \boldsymbol{C}(u)) \end{cases} \tag{6}$$

According to $\boldsymbol{Or}'(u)$ and $\boldsymbol{Or}''(u)$, the tangential, binormal, and normal vectors of the tool-orientation motion can be obtained as

$$\begin{cases} \boldsymbol{T}_{ori}(u) = \dfrac{\boldsymbol{Or}'(u)}{\|\boldsymbol{Or}'(u)\|} \\ \boldsymbol{B}_{ori}(u) = \dfrac{\boldsymbol{Or}'(u) \times \boldsymbol{Or}''(u)}{\|\boldsymbol{Or}'(u) \times \boldsymbol{Or}''(u)\|} \\ \boldsymbol{N}_{ori}(u) = \dfrac{\boldsymbol{Or}'(u) \times \boldsymbol{Or}''(u) \times \boldsymbol{Or}'(u)}{\|\boldsymbol{Or}'(u) \times \boldsymbol{Or}''(u) \times \boldsymbol{Or}'(u)\|} \end{cases} \tag{7}$$

Next, the geometrics of pseudo curves of translational axes and rotary axes are derived based on above information. For a definite motion position, the relationship between the workpiece coordinate and the joint space coordinate can be expressed using the Jacobi matrix as

$$\begin{bmatrix} \boldsymbol{C}' \\ \boldsymbol{Or}' \end{bmatrix} = \underbrace{\begin{bmatrix} \boldsymbol{J}_1 & \boldsymbol{J}_2 \\ \boldsymbol{J}_3 & \boldsymbol{J}_4 \end{bmatrix}}_{\boldsymbol{J}_{6\times5}} \begin{bmatrix} \boldsymbol{q}'_{trans} \\ \boldsymbol{q}'_{rot} \end{bmatrix} \tag{8}$$

$$\text{Above, } \boldsymbol{J}_1 = \begin{bmatrix} \frac{\partial \boldsymbol{C}(1)}{\partial \boldsymbol{q}(1)} & \frac{\partial \boldsymbol{C}(1)}{\partial \boldsymbol{q}(2)} & \frac{\partial \boldsymbol{C}(1)}{\partial \boldsymbol{q}(3)} \\ \frac{\partial \boldsymbol{C}(2)}{\partial \boldsymbol{q}(1)} & \frac{\partial \boldsymbol{C}(2)}{\partial \boldsymbol{q}(2)} & \frac{\partial \boldsymbol{C}(2)}{\partial \boldsymbol{q}(3)} \\ \frac{\partial \boldsymbol{C}(3)}{\partial \boldsymbol{q}(1)} & \frac{\partial \boldsymbol{C}(3)}{\partial \boldsymbol{q}(2)} & \frac{\partial \boldsymbol{C}(2)}{\partial \boldsymbol{q}(3)} \end{bmatrix}, \ \boldsymbol{J}_2 = \begin{bmatrix} \frac{\partial \boldsymbol{C}(1)}{\partial \boldsymbol{q}(4)} & \frac{\partial \boldsymbol{C}(1)}{\partial \boldsymbol{q}(5)} \\ \frac{\partial \boldsymbol{C}(2)}{\partial \boldsymbol{q}(4)} & \frac{\partial \boldsymbol{C}(2)}{\partial \boldsymbol{q}(5)} \\ \frac{\partial \boldsymbol{C}(3)}{\partial \boldsymbol{q}(4)} & \frac{\partial \boldsymbol{C}(3)}{\partial \boldsymbol{q}(5)} \end{bmatrix},$$

$$\boldsymbol{J}_3 = \begin{bmatrix} \frac{\partial \boldsymbol{Or}(1)}{\partial \boldsymbol{q}(1)} & \frac{\partial \boldsymbol{Or}(1)}{\partial \boldsymbol{q}(2)} & \frac{\partial \boldsymbol{Or}(1)}{\partial \boldsymbol{q}(3)} \\ \frac{\partial \boldsymbol{Or}(2)}{\partial \boldsymbol{q}(1)} & \frac{\partial \boldsymbol{Or}(2)}{\partial \boldsymbol{q}(2)} & \frac{\partial \boldsymbol{Or}(3)}{\partial \boldsymbol{q}(3)} \\ \frac{\partial \boldsymbol{Or}(3)}{\partial \boldsymbol{q}(1)} & \frac{\partial \boldsymbol{Or}(3)}{\partial \boldsymbol{q}(2)} & \frac{\partial \boldsymbol{Or}(3)}{\partial \boldsymbol{q}(3)} \end{bmatrix}, \ \boldsymbol{J}_4 = \begin{bmatrix} \frac{\partial \boldsymbol{Or}(1)}{\partial \boldsymbol{q}(4)} & \frac{\partial \boldsymbol{Or}(1)}{\partial \boldsymbol{q}(5)} \\ \frac{\partial \boldsymbol{Or}(2)}{\partial \boldsymbol{q}(4)} & \frac{\partial \boldsymbol{Or}(2)}{\partial \boldsymbol{q}(5)} \\ \frac{\partial \boldsymbol{Or}(3)}{\partial \boldsymbol{q}(4)} & \frac{\partial \boldsymbol{Or}(3)}{\partial \boldsymbol{q}(5)} \end{bmatrix}, \ \boldsymbol{q}_{trans} = [\boldsymbol{q}(1), \boldsymbol{q}(2), \boldsymbol{q}(3)]^T$$

represents the coordinates of three translational axes, and $\boldsymbol{q}_{rot} = [\boldsymbol{q}(4), \boldsymbol{q}(5)]^T$ means the coordinates of two rotary axes. Since the tool orientation $\boldsymbol{Or}$ in workpiece space is determined by merely two rotary axes but has no relationship with translational axes, we have

$$\boldsymbol{J}_3 = \begin{bmatrix} \frac{\partial \boldsymbol{Or}(1)}{\partial \boldsymbol{q}(1)} & \frac{\partial \boldsymbol{Or}(1)}{\partial \boldsymbol{q}(2)} & \frac{\partial \boldsymbol{Or}(1)}{\partial \boldsymbol{q}(3)} \\ \frac{\partial \boldsymbol{Or}(2)}{\partial \boldsymbol{q}(1)} & \frac{\partial \boldsymbol{Or}(2)}{\partial \boldsymbol{q}(2)} & \frac{\partial \boldsymbol{Or}(3)}{\partial \boldsymbol{q}(3)} \\ \frac{\partial \boldsymbol{Or}(3)}{\partial \boldsymbol{q}(1)} & \frac{\partial \boldsymbol{Or}(3)}{\partial \boldsymbol{q}(2)} & \frac{\partial \boldsymbol{Or}(3)}{\partial \boldsymbol{q}(3)} \end{bmatrix} = \boldsymbol{O}_{3\times3} \tag{9}$$

Substituting Eq. (9) to Eq. (8), it can be derived that

$$\begin{cases} \boldsymbol{C}' = \boldsymbol{J}_1 \boldsymbol{q}'_{trans} + \boldsymbol{J}_2 \boldsymbol{q}'_{rot} \\ \boldsymbol{Or}' = \boldsymbol{J}_4 \boldsymbol{q}'_{rot} \end{cases} \tag{10}$$

According to Eq. (10), we can calculate the first and second order derivative vectors of translational-axis and rotary-axis pseudo curves at a definite motion position as

$$\begin{cases} \boldsymbol{q}'_{rot} = \boldsymbol{J}_4^{-1} \boldsymbol{Or}' \\ \boldsymbol{q}''_{rot} = \boldsymbol{J}_4^{-1} \boldsymbol{Or}'' \\ \boldsymbol{q}'_{trans} = \boldsymbol{J}_1^{-1} [\boldsymbol{C}' - \boldsymbol{J}_2 \boldsymbol{q}'_{rot}] \\ \boldsymbol{q}''_{trans} = \boldsymbol{J}_1^{-1} [\boldsymbol{C}'' - \boldsymbol{J}_2 \boldsymbol{q}''_{rot}] \end{cases} \tag{11}$$

The unit normal vectors of two pseudo curves denoted by $\boldsymbol{N}_{trans} \in \mathbb{R}^3$ and $\boldsymbol{N}_{rot} \in \mathbb{R}^2$ which are important in the following can thus be computed by

$$\begin{cases} \boldsymbol{N}_{trans} = \dfrac{\boldsymbol{q}'_{trans} \times \boldsymbol{q}''_{trans} \times \boldsymbol{q}'_{trans}}{\left\|\boldsymbol{q}'_{trans} \times \boldsymbol{q}''_{trans} \times \boldsymbol{q}'_{trans}\right\|} \\ \begin{bmatrix} \boldsymbol{N}_{rot} \\ 0 \end{bmatrix} = \dfrac{\begin{bmatrix} \boldsymbol{q}'_{rot} \\ 0 \end{bmatrix} \times \begin{bmatrix} \boldsymbol{q}''_{rot} \\ 0 \end{bmatrix} \times \begin{bmatrix} \boldsymbol{q}'_{rot} \\ 0 \end{bmatrix}}{\left\| \begin{bmatrix} \boldsymbol{q}'_{rot} \\ 0 \end{bmatrix} \times \begin{bmatrix} \boldsymbol{q}''_{rot} \\ 0 \end{bmatrix} \times \begin{bmatrix} \boldsymbol{q}'_{rot} \\ 0 \end{bmatrix} \right\|} \end{cases} \tag{12}$$

Besides, the curvatures of two pseudo curves, denoted by κ_{trans} and κ_{rot} can be computed as

$$\begin{cases} \kappa_{trans} = \dfrac{\sqrt{\|\boldsymbol{q}'_{trans}\|^2 \|\boldsymbol{q}''_{trans}\|^2 - \left((\boldsymbol{q}'_{trans})^T \boldsymbol{q}''_{trans}\right)^2}}{\|\boldsymbol{q}'_{trans}\|^3} \\ \kappa_{rot} = \dfrac{\sqrt{\|\boldsymbol{q}'_{rot}\|^2 \|\boldsymbol{q}''_{rot}\|^2 - \left((\boldsymbol{q}'_{rot})^T \boldsymbol{q}''_{rot}\right)^2}}{\|\boldsymbol{q}'_{rot}\|^3} \end{cases} \tag{13}$$

Above geometric information of the two pseudo curves will be utilized in the following processes.

2.2.2. Axis-kinematics constrained feedrate modeling

In this section, the tooltip feedrate values constrained by five axes velocity, acceleration, and jerk limits are modeled. Note that the iteration is not used here because there is no need to consider the tangential continuous of the tooltip feedrate in the current step, and the continuous will be ensured in the following filtering step.

(1) Axis-velocity constrained tooltip feedrate

It can be seen from Eq. (1) that the relationship between axis and tooltip velocities is linear, therefore, the first formula in Eq. (1), i.e., $\boldsymbol{v}_{axis} = \boldsymbol{q}_s v_{tip}$, is used to model the axis-velocity constrained tooltip feedrate which is denoted by $v_{tip,\ v}$. Hence, the problem is transformed as the calculation of $\boldsymbol{q}_s$. With the help of differential geometry, we have,

$$v_{tip} = \left\|\frac{d\boldsymbol{C}(u)}{dt}\right\| = \left\|\frac{d\boldsymbol{C}(u)}{du} \bullet \frac{du}{ds} \bullet \frac{ds}{dt}\right\| = \|\boldsymbol{C}'(u)\| \left|\frac{du}{ds}\right| v_{tip} \tag{14}$$

and

$$|\boldsymbol{q}_s| = \left|\frac{d\boldsymbol{q}(u)}{ds}\right| = \left|\frac{d\boldsymbol{q}(u)}{du}\right| \bullet \left|\frac{du}{ds}\right| \tag{15}$$

From Eq. (14), it is seen that $\left|\frac{du}{ds}\right| = \frac{1}{\|\boldsymbol{C}'(u)\|}$, and by substituting it to Eq. (15), we have

$$|\boldsymbol{q}_s| = \frac{\left|\frac{d\boldsymbol{q}(u)}{du}\right|}{\|\boldsymbol{C}'(u)\|} \tag{16}$$

Above, $\boldsymbol{q}(u)$ is the five-dimensional joint-space pseudo curve which is consisted by the translational axis pseudo curve $\boldsymbol{q}_{trans}(u)$ and the rotary axis pseudo curve $\boldsymbol{q}_{rot}(u)$ that share the parameter u of the workpiece-space tooltip curve $\boldsymbol{C}(u)$. The derivative vector of $\boldsymbol{q}(u)$ with respect to u can thus be computed using Eq. (11) as

$$\frac{d\boldsymbol{q}(u)}{du} = \begin{bmatrix} \boldsymbol{q}'_{trans} \\ \boldsymbol{q}'_{rot} \end{bmatrix} \tag{17}$$

According to the first formula of Eq. (1) and Eqs. (16)–(17), the maximum allowable tooltip feedrate $v_{tip,\ v}$ constrained by five axes velocity limitations which are denoted as $\boldsymbol{v}_{axis,\ max}(i) \in \mathbb{R}^+$, $i = 1, 2, \ldots, 5$, can be computed as

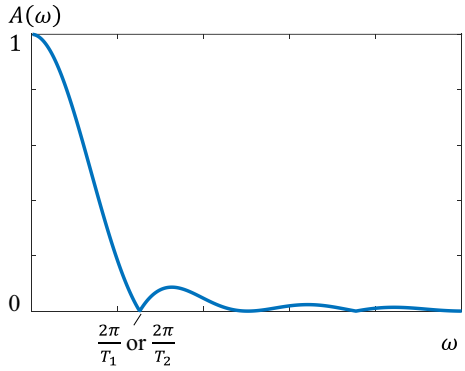

Fig. 2. Magnitude-frequency characteristic of two cascaded FIR filters.

$$v_{tip,v} = \min_{i=1,2,\ldots,5}\left\{\frac{\boldsymbol{v}_{axis,max}(i)}{|\boldsymbol{q}_s(i)|}\right\} = min\left\{\frac{\boldsymbol{v}_{axis,max}(1)}{|\boldsymbol{q}'_{trans}(1)|}, \frac{\boldsymbol{v}_{axis,max}(2)}{|\boldsymbol{q}'_{trans}(2)|}, \frac{\boldsymbol{v}_{axis,max}(3)}{|\boldsymbol{q}'_{trans}(3)|}, \frac{\boldsymbol{v}_{axis,max}(4)}{|\boldsymbol{q}'_{rot}(1)|}, \frac{\boldsymbol{v}_{axis,max}(5)}{|\boldsymbol{q}'_{rot}(2)|}\right\} \bullet \|\boldsymbol{C}'(u)\| \tag{18}$$

For a definite motion position with a definite parameter u, the $\boldsymbol{C}'(u)$ can be obtained using tooltip curve $\boldsymbol{C}(u)$, and the $\boldsymbol{q}_{trans}'$ can be computed by Eq. (11), thus the axis velocity constrained feedrate of the corresponding position can be obtained using Eq. (18).

(2) Axis-acceleration constrained tooltip feedrate

In most existing five-axis feedrate-scheduling methods, the second formula in Eq. (1) is used to obtain the acceleration constrained feedrate, however, the relationship between axis acceleration and tooltip feedrate described by Eq. (1) is nonlinear, which compels the scheduling yield a large margin during the process of inequality equation derivation. In this paper, the pseudo curves are taken as intermediary so that above problem can be solved. Basic idea of the proposed method is introduced below. Since the tooltip motion is realized by translational and rotary axes motions, the relationship between tooltip feedrate and the velocities of the motions on translational-axis pseudo curve and rotary-axis pseudo curve is first established. Then, the maximum acceleration limitations of translational axes and rotary axes are utilized to constrain the two pseudo-curve-point motion velocities. Finally, the allowable tooltip feedrate can be obtained according to the two allowable pseudo-curve-point motion velocities.

It can be easily derived by Eq. (8) that the relationship between tooltip feedrate and pseudo curve motion velocities is

$$v_{tip}\boldsymbol{T}_{tip} = [\boldsymbol{J}_1 \quad \boldsymbol{J}_2]\begin{bmatrix}\boldsymbol{v}_{trans}\\ \boldsymbol{v}_{rot}\end{bmatrix} \tag{19}$$

where $\boldsymbol{v}_{trans}$ and $\boldsymbol{v}_{rot}$ represent the motion velocity vectors of translation-axis pseudo curve and rotary-axis pseudo curve, respectively. Hence, the two pseudo curve motion velocities can be expressed by tooltip feedrate as

$$\begin{cases}\boldsymbol{v}_{trans} = \left([\boldsymbol{J}_1 \quad \boldsymbol{J}_2]^+\boldsymbol{T}_{tip}\right)|_{(1,2,3)}v_{tip}\\ \boldsymbol{v}_{rot} = \left([\boldsymbol{J}_1 \quad \boldsymbol{J}_2]^+\boldsymbol{T}_{tip}\right)|_{(4,5)}v_{tip}\end{cases} \tag{20}$$

Above, $[\boldsymbol{J}_1 \quad \boldsymbol{J}_2]^+$ represents the Moore-Penrose inverse matrix of $[\boldsymbol{J}_1 \quad \boldsymbol{J}_2]$, and it can be computed by $[\boldsymbol{J}_1 \quad \boldsymbol{J}_2]^+ = \begin{bmatrix}\boldsymbol{J}_1^T\\ \boldsymbol{J}_2^T\end{bmatrix}\left[[\boldsymbol{J}_1 \quad \boldsymbol{J}_2]\bullet\begin{bmatrix}\boldsymbol{J}_1^T\\ \boldsymbol{J}_2^T\end{bmatrix}\right]^{-1}$.

For the two pseudo curves, the centripetal accelerations, denoted as a_{trans} for translational-axis pseudo curve and a_{rot} for rotary-axis pseudo curve, can be computed by $a_{trans} = \|\boldsymbol{v}_{trans}\|^2\kappa_{trans}$ and $a_{rot} = \|\boldsymbol{v}_{rot}\|^2\kappa_{rot}$. Accordingly, the axis acceleration limited motion velocities which are denoted as $v_{trans,\,a}$ and $v_{rot,\,a}$, can be solved by

$$\begin{cases}v_{trans,a} = \sqrt{\dfrac{a_{trans,max}}{\kappa_{trans}}}\\ v_{rot,a} = \sqrt{\dfrac{a_{rot,max}}{\kappa_{rot}}}\end{cases} \tag{21}$$

Above, $a_{trans,\,max}$ and $a_{rot,\,max}$ are maximum translational-axis acceleration and maximum rotary-axis acceleration, respectively.

Therefore, if the following inequation

$$\begin{cases}\|\boldsymbol{v}_{trans}\| \le v_{trans,a}\\ \|\boldsymbol{v}_{rot}\| \le v_{rot,a}\end{cases} \tag{22}$$

is satisfied, the five-axis accelerations cannot be exceeded. Thus, the axis acceleration constrained tooltip feedrate which is denoted by $v_{tip,\,a}$ can be solved by synthesize Eqs. (20)–(22) as

$$v_{tip,a} = min\left\{\frac{\sqrt{\frac{a_{trans,max}}{\kappa_{trans}}}}{\left\|\left([\boldsymbol{J}_1 \quad \boldsymbol{J}_2]^+\boldsymbol{T}_{tip}\right)|_{(1,2,3)}\right\|}, \frac{\sqrt{\frac{a_{rot,max}}{\kappa_{rot}}}}{\left\|\left([\boldsymbol{J}_1 \quad \boldsymbol{J}_2]^+\boldsymbol{T}_{tip}\right)|_{(4,5)}\right\|}\right\} \tag{23}$$

In Eq. (23), $(*)|_{(n,p)}$ means a vector constructed by the n-th and p-th elements of the vector (*), additionally, the first and second items in Eq. (23) are tooltip feedrate values constrained by translational-axis acceleration and rotary-axis acceleration limitations, respectively. Note that Eq. (21) is derived according to the centripetal accelerations merely, while the tangential accelerations beyond the centripetal accelerations of pseudo curves also affect the maximum feedrate, but it is not necessarily considered here because the next-step filtering will solve this issue. It should be noticed that if the tangential accelerations were considered here, looking-ahead pre-discretizing or iterative computation would be necessary. This paper releases the consideration of tangential accelerations in this step, so that the pre-processing and iterative computations are not required.

(3) Axis-jerk constrained tooltip feedrate

Similar to the fact that the direction variation of pseudo-curve motion velocities causes centripetal accelerations, the direction variation of centripetal accelerations will also cause the centripetal jerk. Denote j_{trans} and j_{rot} as the centripetal jerks of translational-axis pseudo curve and rotary-axis pseudo curve, respectively, they can be computed by $j_{trans} = \|\boldsymbol{v}_{trans}\|^3\kappa_{trans}^2$ and $j_{rot} = \|\boldsymbol{v}_{rot}\|^3\kappa_{rot}^2$. The detail proof procedure can be found in reference [33]. Therefore, the axis jerks limited motion velocities of the pseudo curves which are denoted by $v_{trans,\,j}$ and $v_{rot,\,j}$, can be solved using the pseudo curvature as

$$\begin{cases}v_{trans,j} = \sqrt[3]{\dfrac{j_{trans,max}}{\kappa_{trans}^2}}\\ v_{rot,j} = \sqrt[3]{\dfrac{j_{rot,max}}{\kappa_{rot}^2}}\end{cases} \tag{24}$$

Above, $j_{trans,\,max}$ and $j_{rot,\,max}$ are maximum translational-axis jerk and maximum rotary-axis jerk, respectively. This proposition has been proofed in most studies related to two-axis or three-axis feedrate scheduling as well.

Therefore, similar to Eq. (23), the axis-jerk constrained tooltip feedrate which is denoted by $v_{tip,\,j}$ can be solved as

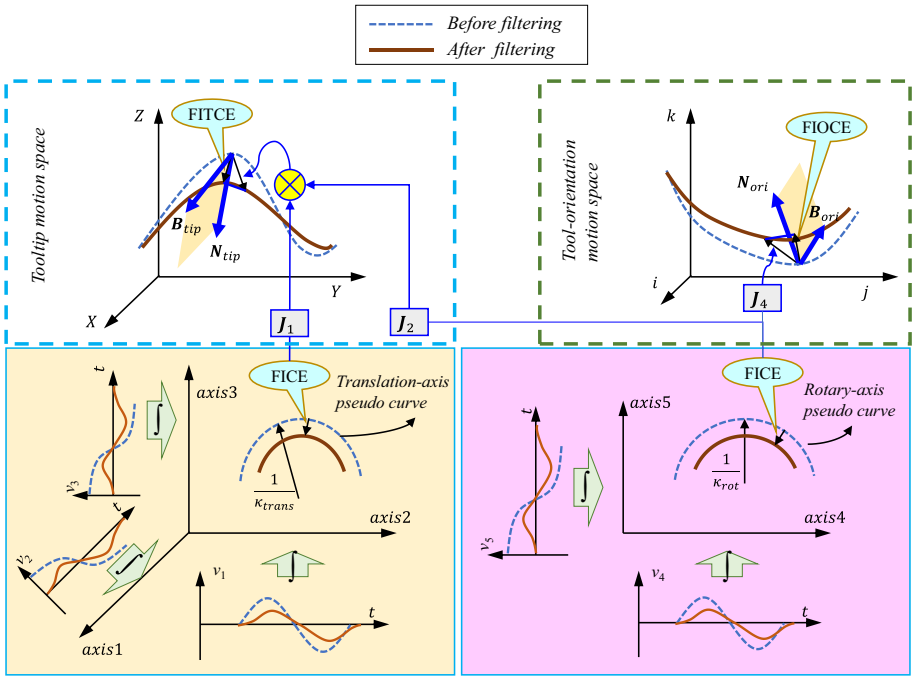

Fig. 3. Illustration of the forming mechanism of five-axis FICEs.

$$v_{tip,j} = min\left\{ \frac{\sqrt[3]{\frac{j_{trans,max}}{\kappa_{trans}^2}}}{\left\| \left([\boldsymbol{J}_1 \quad \boldsymbol{J}_2]^{+} \boldsymbol{T}_{tip} \right)|_{(1,2,3)} \right\|}, \frac{\sqrt[3]{\frac{j_{rot,max}}{\kappa_{rot}^2}}}{\left\| \left([\boldsymbol{J}_1 \quad \boldsymbol{J}_2]^{+} \boldsymbol{T}_{tip} \right)|_{(4,5)} \right\|} \right\} \tag{25}$$

The first and second items in Eq. (25) are tooltip feedrate values constrained by translational-axis jerk and rotary-axis jerk limitations, respectively.

2.2.3. FICE constrained feedrate modeling

For two cascaded FIR filters, the magnitude-frequency characteristic $A(\omega)$ can be expressed as

$$A(\omega) = \frac{4\left|sin\left(\frac{T_1\omega}{2}\right)sin\left(\frac{T_2\omega}{2}\right)\right|}{T_1T_2\omega^2} \tag{26}$$

Above, T_1 and T_2 are two delay constants of the two cascaded FIR filters, and the proof of Eq. (26) can be found in references [27,30]. For intuitive representation, the $A(\omega)$ is plotted in Fig. 2. As can be seen, the magnitude is not larger than 1. Therefore, the magnitudes of motion velocities of all axes will decrease after the filtering operation, which will in sequence induce positional contour errors (FICEs) for translational-axis and rotary-axis pseudo curves. Furthermore, the synthesizing of translational-axis and rotary-axis pseudo-curve FICEs will induce the tooltip contour error FITCE in tooltip motion space, and the rotary-axis pseudo-curve FICE will induce the tool-orientation contour error FIOCE in tool-orientation motion space. Mechanism of above forming process of the filtering-induced five-axis contour errors is illustrated in Fig. 3.

Denote the FICE vectors for translational-axis and rotary-axis pseudo curves as $\boldsymbol{\varepsilon}_{trans}$ and $\boldsymbol{\varepsilon}_{rot}$, respectively. For orthotropic two-axis or three-axis motion, the FICE direction is in line with the normal direction, and the value of FICE $\boldsymbol{\varepsilon}$ can be calculated according to the motion velocity v as

$$\|\boldsymbol{\varepsilon}\| = \frac{\left(T_1^2 + T_2^2\right)\kappa v^2}{24} \tag{27}$$

where κ represents the curvature. Proof of Eq. (27) can be found in our previous studies [29,30]. Therefore, the FICEs of the pseudo curves $\boldsymbol{\varepsilon}_{trans}$ and $\boldsymbol{\varepsilon}_{rot}$ can be computed as

$$\begin{cases} \boldsymbol{\varepsilon}_{trans} = \dfrac{\left(T_1^2 + T_2^2\right)\kappa_{trans}\left\| \left([\boldsymbol{J}_1 \quad \boldsymbol{J}_2]^{+} \boldsymbol{T}_{tip} \right)|_{(1,2,3)} \right\|^2 v_{tip}^2 \boldsymbol{N}_{trans}}{24} \\ \boldsymbol{\varepsilon}_{rot} = \dfrac{\left(T_1^2 + T_2^2\right)\kappa_{rot}\left\| \left([\boldsymbol{J}_1 \quad \boldsymbol{J}_2]^{+} \boldsymbol{T}_{tip} \right)|_{(4,5)} \right\|^2 v_{tip}^2 \boldsymbol{N}_{rot}}{24} \end{cases} \tag{28}$$

Denote the FITCE in the tooltip motion space as $\boldsymbol{\varepsilon}_{tip}$, and as shown in Fig. 3, both $\boldsymbol{\varepsilon}_{trans}$ and $\boldsymbol{\varepsilon}_{rot}$ have contribute to $\boldsymbol{\varepsilon}_{tip}$. After transforming $\boldsymbol{\varepsilon}_{trans}$ and $\boldsymbol{\varepsilon}_{rot}$ from joint space to tooltip space thus obtaining a tooltip motion error vector, its projection on the normal plane of the tooltip motion contour will be the FITCE. Therefore, the $\boldsymbol{\varepsilon}_{tip}$ can be computed by

$$\boldsymbol{\varepsilon}_{tip} = Proj_{N_t}\left([\boldsymbol{J}_1 \quad \boldsymbol{J}_2] \begin{bmatrix} \boldsymbol{\varepsilon}_{trans} \\ \boldsymbol{\varepsilon}_{rot} \end{bmatrix} \right) = \boldsymbol{N}_t\left(\boldsymbol{N}_t^T\boldsymbol{N}_t\right)^{-1}\boldsymbol{N}_t^T[\boldsymbol{J}_1 \quad \boldsymbol{J}_2] \begin{bmatrix} \boldsymbol{\varepsilon}_{trans} \\ \boldsymbol{\varepsilon}_{rot} \end{bmatrix} \tag{29}$$

Above, $Proj_{N_t}(*)$ stands for the projection of the vector * on the normal plane of the tooltip contour, and the matrix $\boldsymbol{N}_t$ is consisted by the normal and binormal vectors as $\boldsymbol{N}_t = [\boldsymbol{N}_{tip}, \boldsymbol{B}_{tip}]$.

Denote the FIOCE in the tool-orientation motion space as $\boldsymbol{\varepsilon}_{ori}$, and as shown in Fig. 3, merely $\boldsymbol{\varepsilon}_{rot}$ has contribute to $\boldsymbol{\varepsilon}_{ori}$. After transforming $\boldsymbol{\varepsilon}_{rot}$ from joint space to tool-orientation space thus obtaining a tool-orientation motion error vector, its projection on the normal plane of the tool-orientation motion contour will be the FITCE. Therefore, the $\boldsymbol{\varepsilon}_{ori}$ can be computed by

$$\boldsymbol{\varepsilon}_{ori} = Proj_{N_o}(\boldsymbol{J}_4\boldsymbol{\varepsilon}_{rot}) = \boldsymbol{N}_o\left(\boldsymbol{N}_o^T\boldsymbol{N}_o\right)^{-1}\boldsymbol{N}_o^T\boldsymbol{J}_4\boldsymbol{\varepsilon}_{rot} \tag{30}$$

Above, $Proj_{N_o}(*)$ stands for the projection of the vector * on the normal plane of the tool-orientation contour, and the matrix $\boldsymbol{N}_o$ is consisted by the normal and binormal vectors as $\boldsymbol{N}_o = [\boldsymbol{N}_{ori}, \boldsymbol{B}_{ori}]$.

Given the maximum allowable FITCE and FIOCE as $\varepsilon_{tip,\ max}$ and $\varepsilon_{ori,\ max}$, respectively, the maximum allowable tooltip feedrate corresponding to $\varepsilon_{tip,\ max}$ and $\varepsilon_{ori,\ max}$ can be computed using Eqs. (28)–(30) by letting $\|\boldsymbol{\varepsilon}_{tip}\| = \varepsilon_{tip,\ max}$ and $\|\boldsymbol{\varepsilon}_{ori}\| = \varepsilon_{ori,\ max}$. Denoting the FITCE and FIOCE constrained tooltip feedrate values as $v_{tip,\ et}$ and $v_{tip,\ eo}$, respectively, they can be derived as

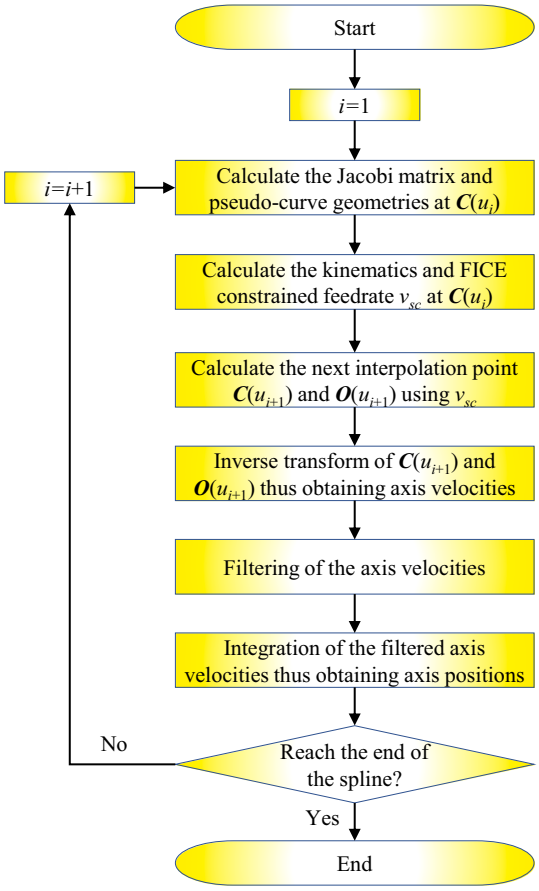

Fig. 4. Procedure of the proposed five-axis dual-spline interpolation method.

$$v_{tip,et}=\sqrt{\frac{24\varepsilon_{tip,max}}{\left(T_1^2+T_2^2\right)\left\|\boldsymbol{N}_t\left(\boldsymbol{N}_t^T\boldsymbol{N}_t\right)^{-1}\boldsymbol{N}_t^T[\boldsymbol{J}_1\boldsymbol{J}_2]\begin{bmatrix}\kappa_{trans}\left\|\left([\boldsymbol{J}_1\boldsymbol{J}_2]^+\boldsymbol{T}_{tip}\right)|_{(1,2,3)}\right\|^2\boldsymbol{N}_{trans}\\ \kappa_{rot}\left\|\left([\boldsymbol{J}_1\boldsymbol{J}_2]^+\boldsymbol{T}_{tip}\right)|_{(4,5)}\right\|^2\boldsymbol{N}_{rot}\end{bmatrix}\right\|}} \tag{31}$$

and

$$v_{tip,eo}=\sqrt{\frac{24\varepsilon_{ori,max}}{\left(T_1^2+T_2^2\right)\left\|\boldsymbol{N}_o\left(\boldsymbol{N}_o^T\boldsymbol{N}_o\right)^{-1}\boldsymbol{N}_o^T\boldsymbol{J}_4\kappa_{rot}\left\|\left([\boldsymbol{J}_1\quad\boldsymbol{J}_2]^+\boldsymbol{T}_{tip}\right)|_{(4,5)}\right\|^2\boldsymbol{N}_{rot}\right\|}} \tag{32}$$

Note that above FICE constrained feedrate models are based on the condition that the error increases with the rising of feedrate, which means that the magnitude should decreases with the rising of the frequency or feedrate. To satisfy this condition, the Fig. 2 shows that we must let the translational-axis and rotary-axis pseudo-curve motion velocities, or frequencies, satisfy the following inequations

$$\begin{cases}\omega_{trans}=\kappa_{trans}\|\boldsymbol{v}_{trans}\|\le min\left\{\dfrac{2\pi}{T_1},\dfrac{2\pi}{T_2}\right\}\\ \omega_{rot}=\kappa_{rot}\|\boldsymbol{v}_{rot}\|\le min\left\{\dfrac{2\pi}{T_1},\dfrac{2\pi}{T_2}\right\}\end{cases} \tag{33}$$

These two inequations in Eq. (33) propose additive frequency constraints for the tooltip feedrate which is denoted by $v_{tip,\,fq}$, and it can be computed according to Eq. (20) and Eq. (33) as

$$v_{tip,fq}=min\left\{\frac{min\left\{\frac{2\pi}{T_1},\frac{2\pi}{T_2}\right\}}{\kappa_{trans}\left\|\left([\boldsymbol{J}_1\quad\boldsymbol{J}_2]^+\boldsymbol{T}_{tip}\right)|_{(1,2,3)}\right\|},\frac{min\left\{\frac{2\pi}{T_1},\frac{2\pi}{T_2}\right\}}{\kappa_{rot}\left\|\left([\boldsymbol{J}_1\quad\boldsymbol{J}_2]^+\boldsymbol{T}_{tip}\right)|_{(4,5)}\right\|}\right\} \tag{34}$$

Hence, the five-axis FICEs introduce three kinds of maximum allowable tooltip feedrate, i.e., the FITCE constrained feedrate $v_{tip,\,et}$, the FIOCE constrained feedrate $v_{tip,\,eo}$, and the frequency constrained feedrate $v_{tip,\,fq}$. They can be computed by Eq. (31), Eq. (32), and Eq. (34), respectively.

2.2.4. Generation of the axis positions in each interpolation period

For a definite interpolation point, the scheduled feedrate can be computed by combination of above-mentioned constraints as

$$v_{sc}=min\left\{v_p,v_{tip,v},v_{tip,a},v_{tip,j},v_{tip,et},v_{tip,eo},v_{tip,fq}\right\} \tag{35}$$

Above, v_{sc} represents the scheduled tooltip feedrate, and v_p represents the programmed maximum tooltip feedrate. According to the scheduled tooltip feedrate, the next-interpolation-point parameter u_{i+1} of the dual-spline toolpath is calculated based on the typical second-order Runge-Kutta method [33] as

$$u_{i+1}=u_i+\frac{T_s}{2}(k_1+k_2) \tag{36}$$

where T_s stands for the interpolation period, and the parameters k_1 and k_2 are computed by

$$\begin{cases}k_1=\dfrac{v_{sc,i}}{\|\boldsymbol{C}'(u_i)\|}\\ k_2=\dfrac{v_{sc,i}}{\|\boldsymbol{C}'(u_i+T_sk_1)\|}\end{cases} \tag{37}$$

where $v_{sc,\,i}$ represents the scheduled tooltip feedrate corresponding to the current interpolation point whose parameter is denoted as u_i.

According to the parameter u_{i+1}, the five-dimensional joint-space axis motion positions $\boldsymbol{q}^{i+1}$ can be obtained by inverse transformation of five-axis machine tools as

$$\boldsymbol{q}^{i+1}=Inv\_Trans(\boldsymbol{C}(u_{i+1}),\boldsymbol{Or}(u_{i+1})) \tag{38}$$

The axis motion velocities before filtering can be obtained as

$$\boldsymbol{v}_{axis}^i=\begin{bmatrix}\boldsymbol{v}_{trans}^i\\ \boldsymbol{v}_{rot}^i\end{bmatrix}=\frac{\boldsymbol{q}^{i+1}-\boldsymbol{q}^i}{T_s} \tag{39}$$

After that, the axis motion velocities are filtered by two cascaded FIR filters. Applying convolution with two FIR filters for $\boldsymbol{v}_{axis}^i$ yields the filtered axis motion velocity vector. In discrete domain, the filtered axis motion velocity vector can be computed by [32].

$$\begin{cases}\boldsymbol{v}_{axis,f1}^i=\boldsymbol{v}_{axis,f1}^{i-1}+\dfrac{1}{N_1}\left(\boldsymbol{v}_{axis}^i-\boldsymbol{v}_{axis}^{i-N_1}\right),N_1=int\left(\dfrac{T_1}{T_s}\right)\\ \boldsymbol{v}_{axis,f2}^i=\boldsymbol{v}_{axis,f2}^{i-1}+\dfrac{1}{N_2}\left(\boldsymbol{v}_{axis,f1}^i-\boldsymbol{v}_{axis,f1}^{i-N_2}\right),N_2=int\left(\dfrac{T_2}{T_s}\right)\end{cases} \tag{40}$$

Above, $\boldsymbol{v}_{axis,\,f1}^i$ is the axis velocity vector after one-time filtering, and $\boldsymbol{v}_{axis,\,f2}^i$ is the final axis velocity vector after two-time filtering. Determination of T_1 and T_2 should meet the axis kinematics limitations. For two adjacent points with velocities v_{former} and v_{latter}, the filtered velocity v can be expressed as a function with respect to time t:

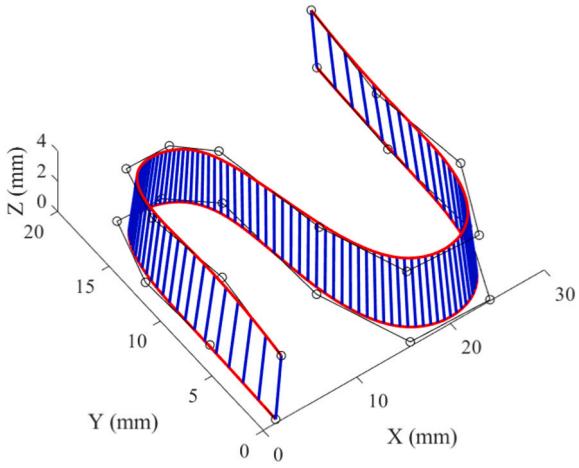

Fig. 5. S-shaped dual-spline toolpath.

Table 1
Parameters for the illustration tests.

Symbol	Parameter	Value
v_p	Maximum tooltip feedrate	Unlimited
$v_{trans,\ max}$	Velocity constraint of translational axes	100 mm/s
$v_{rot,\ max}$	Velocity constraint of rotary axes	4 rad/s
$a_{trans,\ max}$	Acceleration constraint of translational axes	2000 mm/s^2
$a_{rot,\ max}$	Acceleration constraint of rotary axes	80 rad/s^2
$j_{trans,\ max}$	Jerk constraint of translational axes	120,000 mm/s^3
$j_{rot,\ max}$	Jerk constraint of rotary axes	4000 rad/s^3
$\varepsilon_{tip,\ max}$	FITCE constraint	Unlimited for test 1; 0.05 mm for test 2
$\varepsilon_{ori,\ max}$	FIOCE constraint	Unlimited for test 1; 0.1 degree for test 2

$$v(t)=\begin{cases} v_{former}+\dfrac{v_{latter}-v_{former}}{T_1T_2}t^2, & 0\le t<T_2 \\ v_{former}+\dfrac{1}{2}\dfrac{(v_{latter}-v_{former})T_2}{T_1}+\dfrac{(v_{latter}-v_{former})}{T_1}(t-T_2), & T_2\le t<T_1 \\ v_{latter}-\dfrac{1}{2}\dfrac{(v_{latter}-v_{former})}{T_1T_2}(T_1+T_2-t)^2, & T_1\le t<T_1+T_2 \\ v_{latter}, & t\ge T_1+T_2 \end{cases} \tag{41}$$

By differentiating Eq. (41), we can obtain the maximum acceleration a_{max} and maximum jerk j_{max} as

$$\begin{cases} a_{max}=\dfrac{|v_{latter}-v_{former}|}{T_1} \\ j_{max}=\dfrac{|v_{latter}-v_{former}|}{T_1T_2} \end{cases} \tag{42}$$

For translational and rotary axes, the maximum velocities as denoted as $v_{trans,\ max}$ and $v_{rot,\ max}$, respectively, therefore, we have $|v_{latter}-v_{former}| \le v_{trans,\ max}$ for translational axes, and $|v_{latter}-v_{former}| \le v_{rot,\ max}$ for rotary axes. Hence, the following conditions should be satisfied to guarantee the maximum accelerations and jerks being confined after filtering.

$$\begin{cases} a_{trans,max}\ge \dfrac{v_{trans,max}}{T_1} \\ a_{rot,max}\ge \dfrac{v_{rot,max}}{T_1} \\ j_{trans,max}\ge \dfrac{v_{trans,max}}{T_1T_2} \\ j_{rot,max}\ge \dfrac{v_{rot,max}}{T_1T_2} \end{cases} \tag{43}$$

For the sake of synchronization of translational axes and rotary axes, the time constants of filters for all axes should be set as the same values. Therefore, the parameters of the filters T_1 and T_2 can be determined according to Eq. (43) as

$$\begin{cases} T_1=max\left\{\dfrac{v_{trans,max}}{a_{trans,max}},\ \dfrac{v_{rot,max}}{a_{rot,max}}\right\} \\ T_2=max\left\{\dfrac{v_{trans,max}}{T_1j_{trans,max}},\ \dfrac{v_{rot,max}}{T_1j_{rot,max}}\right\} \end{cases} \tag{44}$$

Note that there exists an integral round-off function in Eq. (40), and the reason is explained as follows. The parameters N_1 and N_2 can be computed in light of the FIR filtering principle and the axial drive constraints in theory, but if the theoretical values are not integers, the filter cannot be realized in real application because of the fixed sampling and interpolation period. If T_1 and T_2 are not integral multiple of the interpolation period T_s, they cannot be realized physically. Therefore, T_1 and T_2 are amended as the closest values to their theoretical values by applying the integral function to N_1 and N_2, so that the amended values can meet both of the axial drive requirements and the integral multiple of the interpolation period T_s.

Integrating the final filtered axis velocities in $\boldsymbol{v}^i_{axis,\ f2}$ yields the corresponding axis motion positions. These positions are final outputs of the proposed interpolation algorithm in i-th interpolation loop. Continue the interpolation to $(i+1)$-th interpolation loop until the end of the dual-spline toolpath is reached, thus completing the whole interpolation. Procedure of the interpolation algorithm is concluded in Fig. 4. It can be seen that each step can be finished in one or several equations, and the iterative computation is not required within each interpolation loop, which is one of the benefits of the proposed method.

3. Verification tests

This section conducts illustration tests and experimental tests to verify the feasibility of the proposed five-axis dual-spline interpolation method. Comparison results with existing method is also illustrated to evaluate the advantage performances.

3.1. Illustration tests

A typical S-shaped dual-spline toolpath shown in Fig. 5 which is always used for testing the performances of five-axis machine tools is employed here to illustrate the effectiveness of the proposed method. A five-axis machine tool with three translational axes X/Y/Z and two rotary axes B/C is adopted as the testing objective. The direct and inverse kinematics transformations are

$$\begin{cases} Or_x=sin(q_b)cos(q_c) \\ Or_y=-sin(q_b)sin(q_c) \\ Or_z=cos(q_b) \\ C_x=-sin(q_b)cos(q_c)L+cos(q_c)(q_x-M_x)+sin(q_c)(q_y-M_y)+M_x \\ C_y=sin(q_b)sin(q_c)L-sin(q_c)(q_x-M_x)+cos(\theta_c)(q_y-M_y)+M_y \\ C_z=-cos(q_b)L+q_z+L \end{cases} \tag{45}$$

and

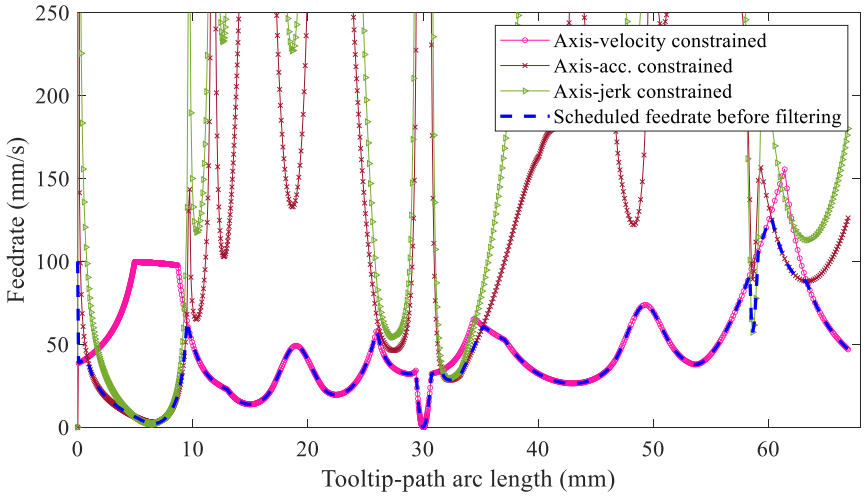

Fig. 6. Multi-item constrained feedrate of test 1.

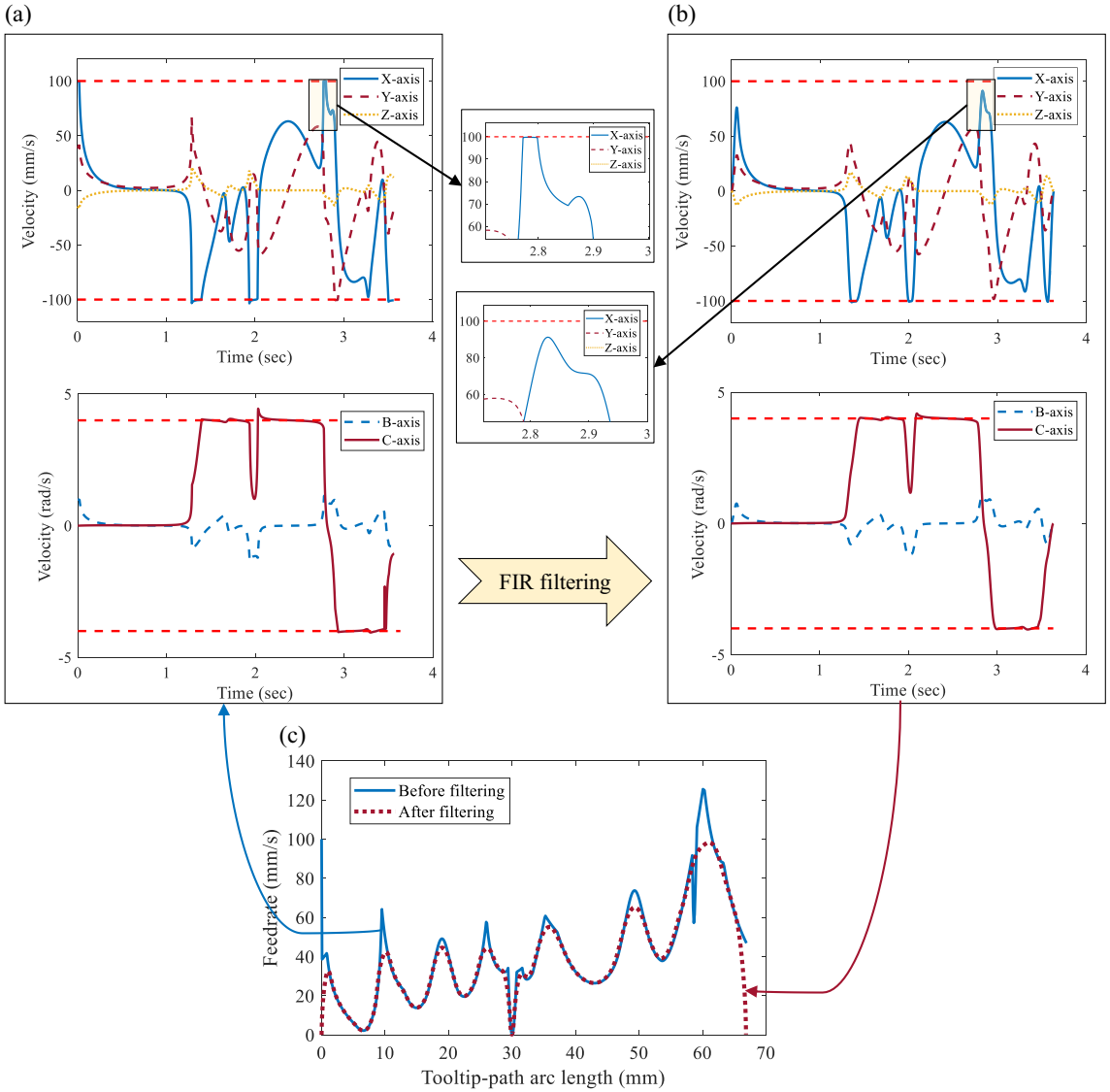

Fig. 7. Axis velocities and feedrate comparison. (a) Axis velocities before filtering. (b) Axis velocities after filtering. (c) Comparison of tooltip feedrate before and after filtering.

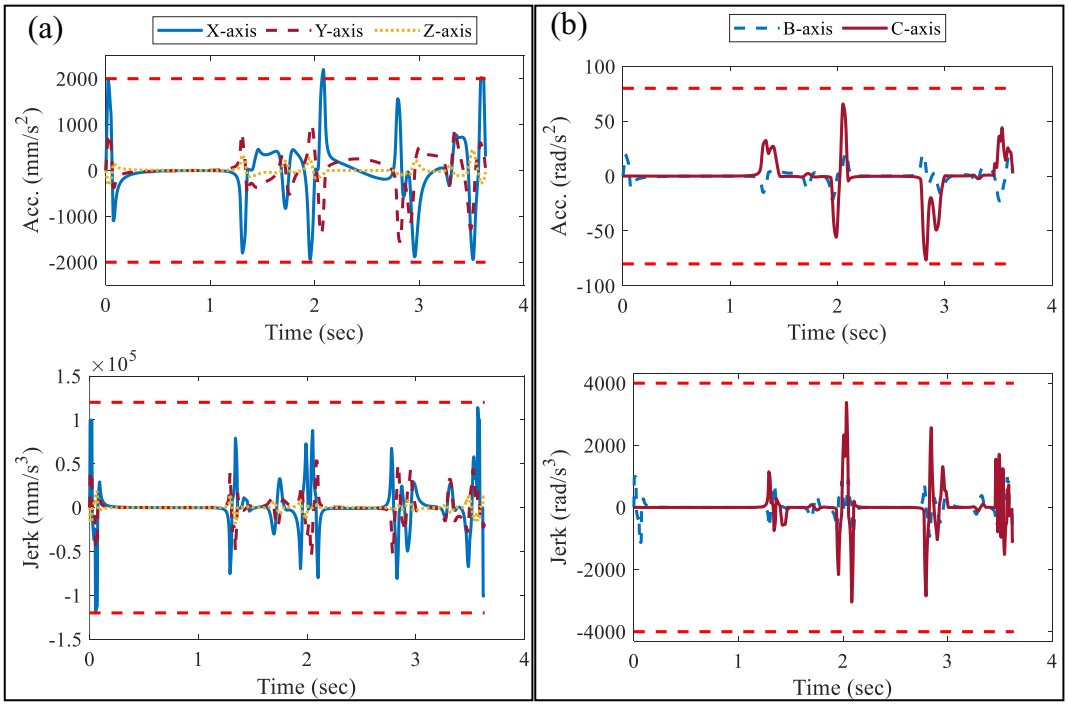

Fig. 8. Actual kinematics of five axes. (a) Accelerations and jerks of translational axes. (b) Accelerations and jerks of rotary axes.

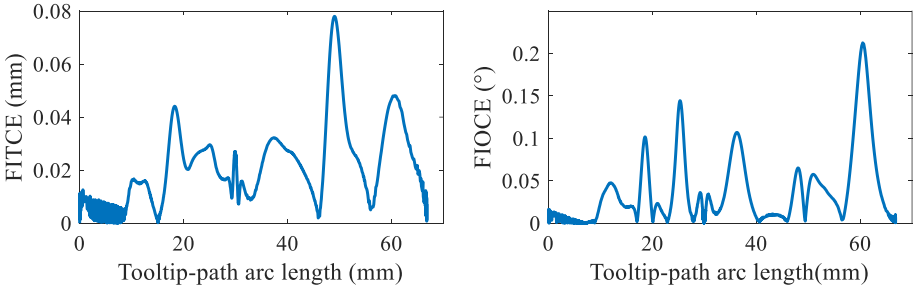

Fig. 9. FITCE and FIOCE of test 1.

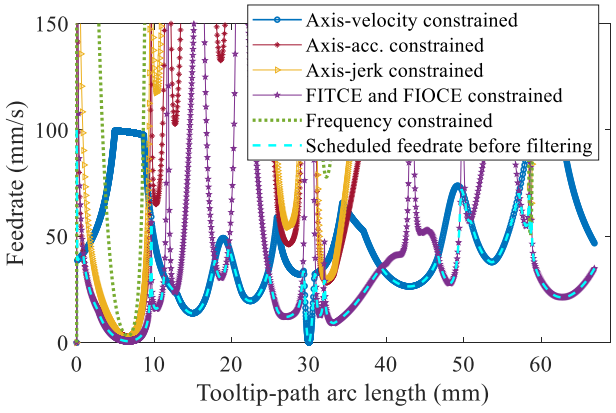

Fig. 10. Multi-item constrained feedrate of test 2.

$$
\begin{cases}
q_b = karccos(Or_z), \ \ k = 1, -1 \\
q_c = \begin{cases} k\pi + arctan\left(Or_x / Or_y\right), \ \ Or_x \neq 0, Or_y \neq 0, k = 0, \pm 1, \pm 2, \cdots \\ 0, \ \ Or_x = 0, Or_y = 0 \\ k\pi/2, Or_x = 0, Or_y \neq 0, k = 0, \pm 1, \cdots \end{cases} \\
q_x = M_x + sin(q_b)L + cos(q_c)(C_x - M_x) - sin(q_c)\left(C_y - M_y\right) \\
q_y = M_y - sin(q_c)(C_x - M_x) + cos(q_c)\left(C_y - M_y\right) \\
q_z = cos(q_b)L - L + C_z
\end{cases}
\tag{46}
$$

respectively. Above, $\boldsymbol{q} = [q_x, q_y, q_z, q_b, q_c]^{\mathrm{T}}$ is the axial position vector; $\boldsymbol{C} = [C_x, C_y, C_z]^{\mathrm{T}}$ and $\boldsymbol{Or} = [Or_x, Or_y, Or_z]^{\mathrm{T}}$ is the tool-tip position and tool-orientation vector, respectively; L represents the distance from the B-axis rotary axis to the tool-tip, and $[M_x, M_y, M_z]^{\mathrm{T}}$ is the origin of the machining coordinate.

According to above kinematics transformation equations, the Jacobi matrix which contains $\boldsymbol{J}_1$, $\boldsymbol{J}_2$, and $\boldsymbol{J}_4$ used in this method can be computed as

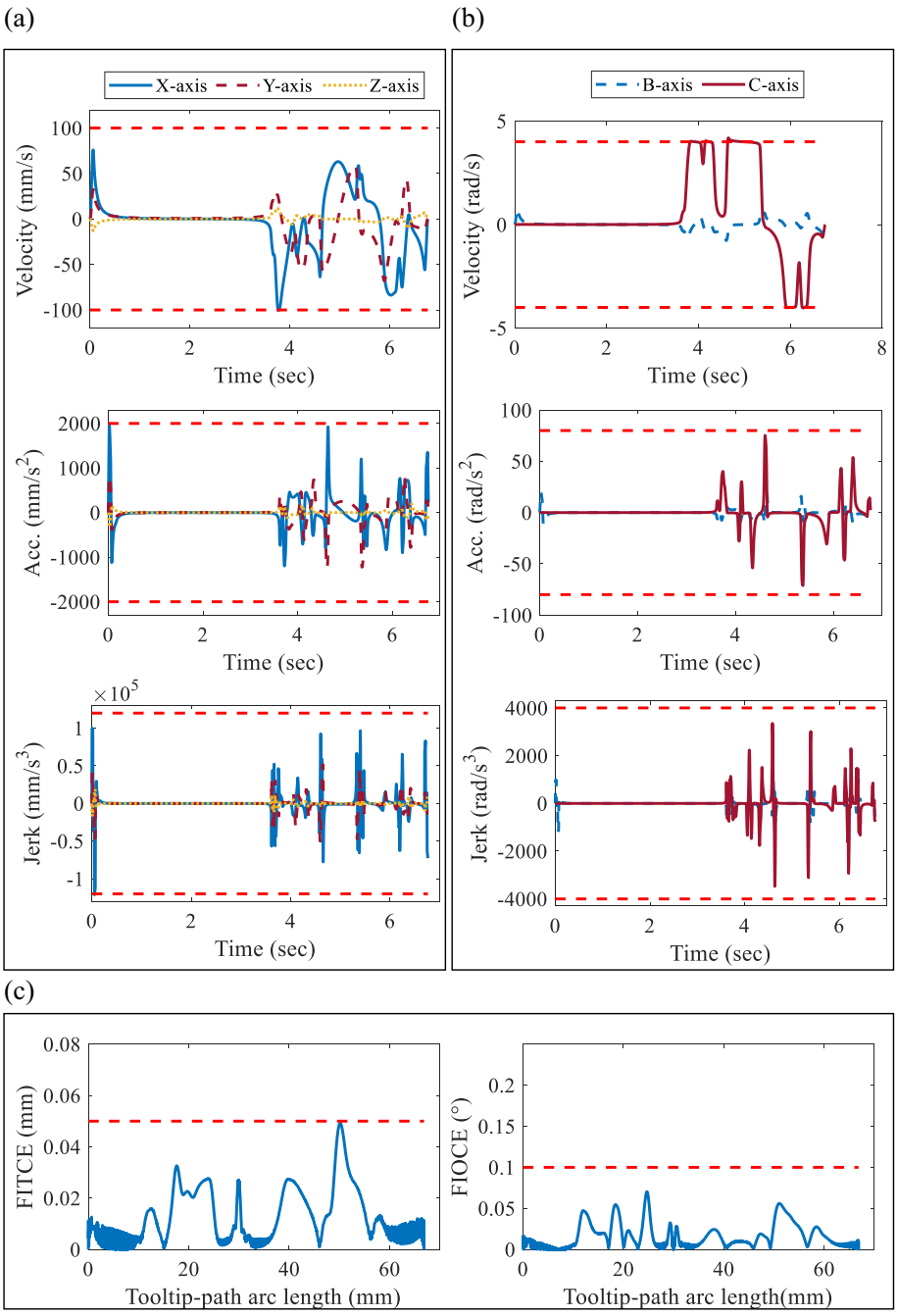

Fig. 11. Axis kinematics and FICE results of test 2. (a) Velocities, accelerations, and jerks of translational axes. (b) Velocities, accelerations, and jerks of rotary axes. (c) Workpiece space FITCE and FIOCE.

$$\boldsymbol{J}_1 = \begin{bmatrix} cos(q_c) & sin(q_c) & 0 \\ -sin(q_c) & cos(q_c) & 0 \\ 0 & 0 & 1 \end{bmatrix} \tag{47}$$

$$\boldsymbol{J}_2 = \begin{bmatrix} -cos(q_b)cos(q_c)L & sin(q_b)sin(q_c)L - sin(q_c)(q_x - M_x) + cos(q_c)(q_y - M_y) \\ cos(q_b)sin(q_c)L & sin(q_b)cos(q_c)L - cos(q_c)(q_x - M_x) - sin(q_c)(q_y - M_y) \\ sin(q_b)L & 0 \end{bmatrix} \tag{48}$$

$$\boldsymbol{J}_4 = \begin{bmatrix} cos(q_b)cos(q_c) & -sin(q_b)sin(q_c) \\ -cos(q_b)sin(q_c) & -sin(q_b)cos(q_c) \\ -sin(q_b) & 0 \end{bmatrix} \tag{49}$$

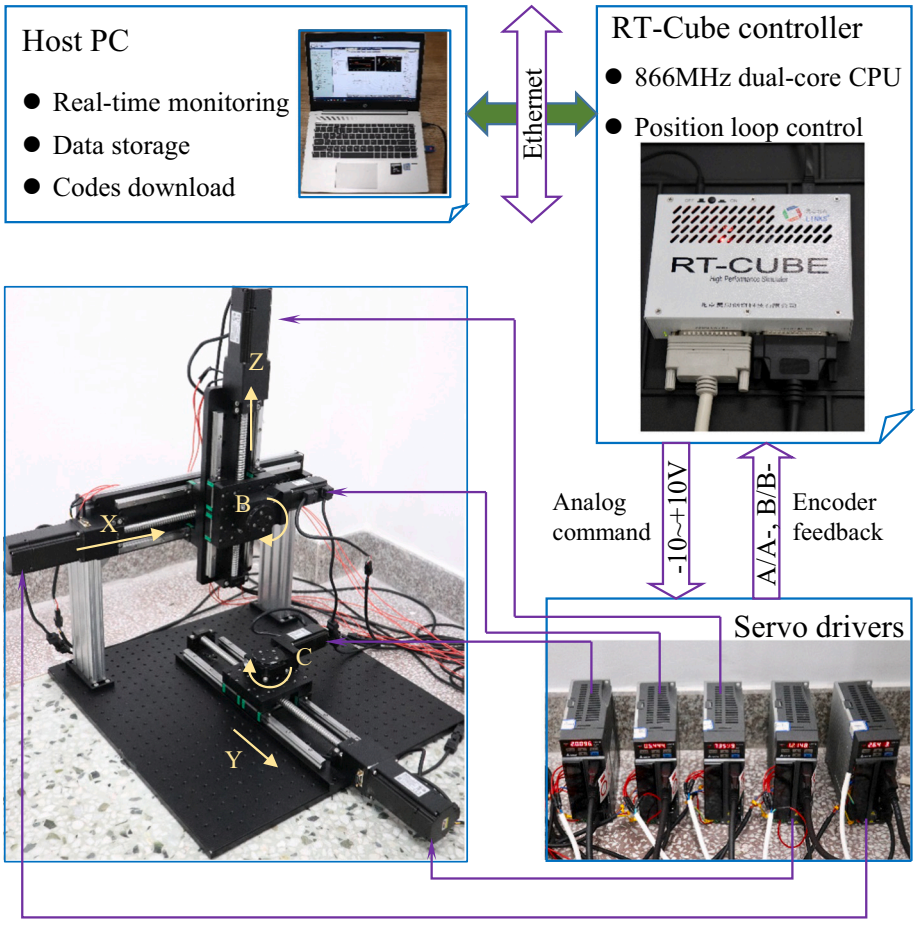

Fig. 12. Experimental setup.

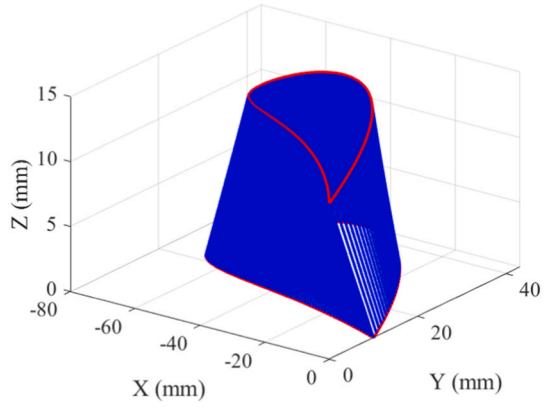

Fig. 13. Blade-shape dual-spline toolpath.

Hence, the geometric characteristics of the pseudo curves at any position can be computed according to the method in Section 3.1. The testing parameters are set as those shown in Table 1. In the first test, the FITCE and FIOCE are not limited so as to verify the effectiveness of the kinematics constrain effect. In the second test, the FITCE and FIOCE limitations are set as 0.05 mm and 0.1 degree, respectively, so as to verify the FICE constrain effect. In both tests, the maximum tooltip feedrate values are not limited, thus, the feedrate can be as large as possible under the considered constraints.

The testing results are illustrated as follows. For the first test which does not set the FICE constraint, the axis-velocity constrained feedrate

Table 2
Parameters for the comparison tests.

Symbol	Parameter	Value
v_p	Maximum tooltip feedrate	40 mm/s
$v_{trans,\ max}$	Velocity constraint of translational axes	40 mm/s
$v_{rot,\ max}$	Velocity constraint of rotary axes	1 rad/s
$a_{trans,\ max}$	Acceleration constraint of translational axes	800 mm/s^2
$a_{rot,\ max}$	Acceleration constraint of rotary axes	20 rad/s^2
$j_{trans,\ max}$	Jerk constraint of translational axes	24,000 mm/s^3
$j_{rot,\ max}$	Jerk constraint of rotary axes	600 rad/s^3
$\varepsilon_{tip,\ max}$	FITCE constraint	0.05 mm
$\varepsilon_{ori,\ max}$	FIOCE constraint	0.1°

$v_{tip,\ v}$, the axis-acceleration constrained feedrate $v_{tip,\ a}$, and the axis-jerk constrained feedrate $v_{tip,\ j}$ are shown in Fig. 6, where the scheduled feedrate v_{sc} which is the minimum value of above limited feedrate values is illustrated together. Using the scheduled feedrate in Fig. 6, velocities of five axes can be generated, and they are shown in Fig. 7(a). After that, these five-axis velocities are filtered separately by two cascaded FIR filters, and the filtered velocities of five axes are shown in Fig. 7(b). As can be seen, the filtered axis velocities are smooth enough. Integrals are applied to the filtered axis velocities for generation of five-axis reference positions which act as the output of the five-axis dual-spline interpolator. Additionally, the real output positions are utilized for calculation of the real tooltip feedrate after filtering, and it is compared with the scheduled feedrate before filtering in Fig. 7(c). In order to verify the effectiveness of the multiple-item constraints, the actual obtained five-axis accelerations and jerks computed by differentiating the output axis positions are illustrated in Fig. 8. As can be seen from Fig. 8, the

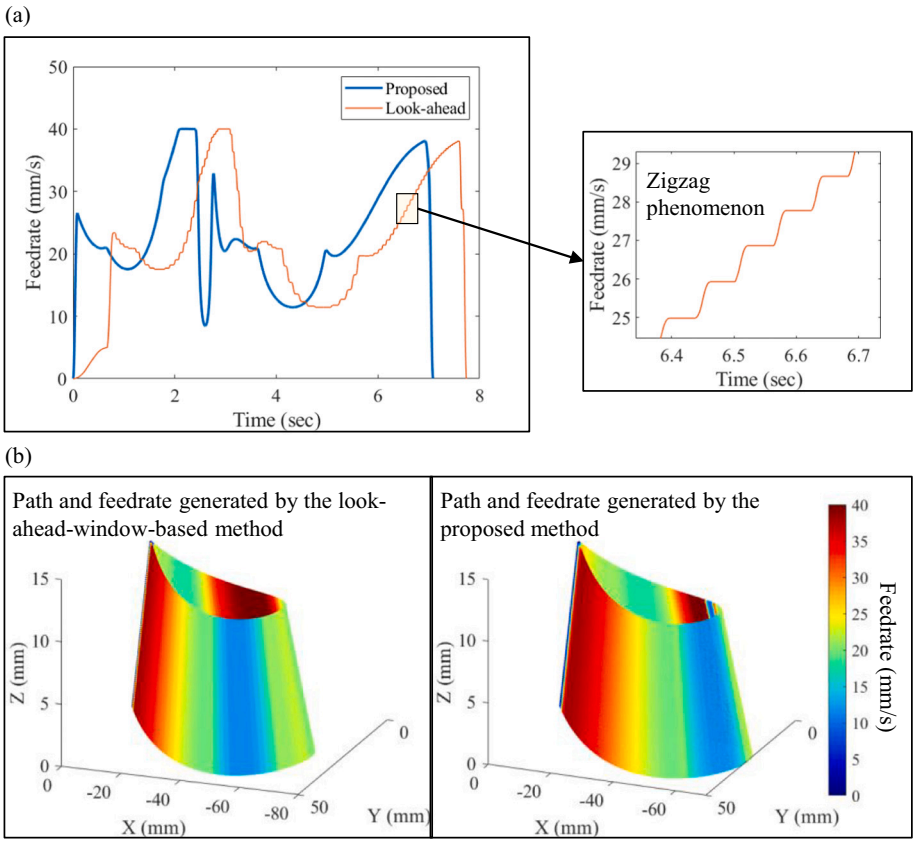

Fig. 14. Tooltip feedrate profiles comparison. (a) Comparison of tooltip feedrate profiles with respect to time. (b) Comparison of tooltip feedrate values on the toolpaths.

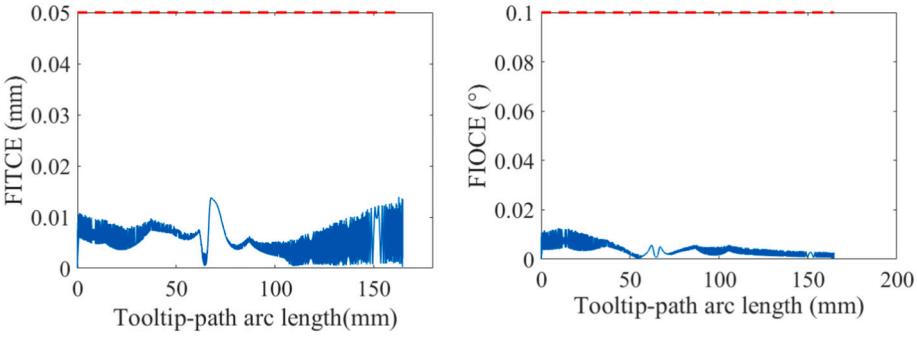

Fig. 15. FITCE and FIOCE of the blade-shape toolpath.

accelerations and jerks of three translational axes and two rotary axes can all be confined within the limitations set in Table 1. Although the acceleration of *x*-axis slightly exceeds the constraint value, the error is less than 3% and the exceeding time is less than 0.01 s, which is acceptable in industrial application. The reasons for the slightly exceeding may be caused by three factors. First, the transaction from pseudo-curve velocities to the tooltip velocity is realized by using the Jacobian matrix which is a first-order approximation matrix. Although the approximation error is extremely small due to the small interpolation period, there exists few errors. Second, the time constant of the FIR filter is derived by continuous model, while in real application the discrete model should be used in NC controller. Although the sampling period is extremely small, there exists a little difference between two kinds of models. Third, the roundoff errors during the comprehensive calculations may also cause the slight exceeding. Nevertheless, the slightly exceeding does not affect the effectiveness and favorable performances of the proposed method.

Although the FITCE and FIOCE are not limited in above test, the actual obtained FITCE and FIOCE of the interpolation toolpath are computed and shown in Fig. 9. The maximum FITCE is about 0.08 mm, and the maximum FIOCE is about 0.22 degree. Although the errors are not very large, we conduct test 2 where the FITCE and FIOCE limitations are set as 0.05 mm and 0.1 degree, respectively, so as to evaluate the performance of the effectiveness of FICE constraint. The multi-item constrained tooltip feedrate values are illustrated in Fig. 10. It can be seen from Fig. 10 that the FITCE and FIOCE constraints become leading constraints in most areas when comparing with kinematics limitations. The final obtained actual axis velocities, axis accelerations, axis jerks, and real FITCE and FIOCE are shown in Fig. 11. As can be seen from Fig. 11, all the parameters containing axis kinematics and workpiece space FITCE and FIOCE can be effectively constrained, which demonstrate the feasibility of the proposed method totally.

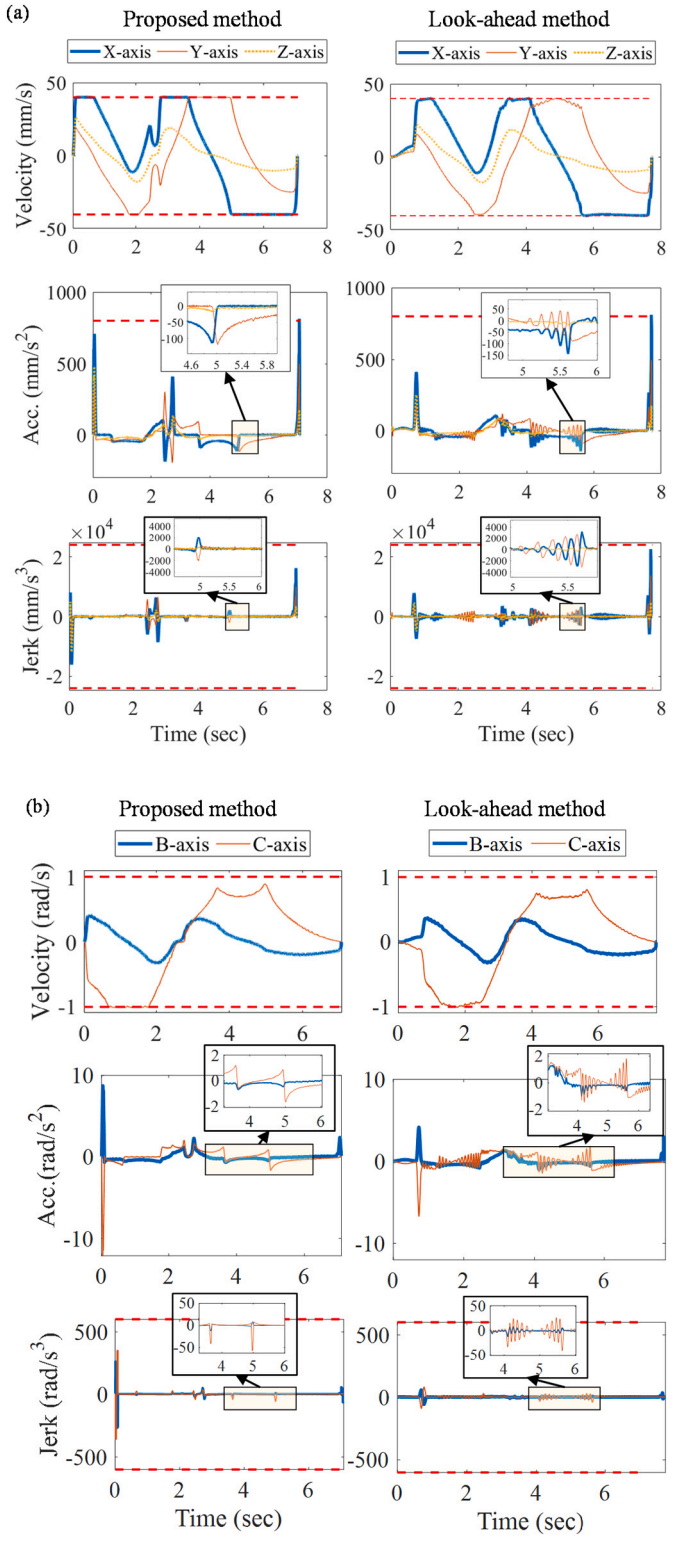

Fig. 16. Comparison of the kinematics parameters. (a) Comparison of translational-axis kinematics. (b) Comparison of rotary-axis kinematics.

3.2. Experimental comparison tests

This section further evaluates the performances of the proposed method by experimental comparison tests. The experiments are conducted on an in-house five-axis feed-drive platform shown in Fig. 12. The five axes contain three translational axes $X/Y/Z$ and two rotary axes B/C which are the same to those set in the illustration tests. Each axis is driven by a DC servo motor. Five servo motors are controlled by an open real-time controller with an 866 MHz dual-core CPU. The position loops of five axes are conducted in this controller. The host-PC is utilized for data monitoring and storage.

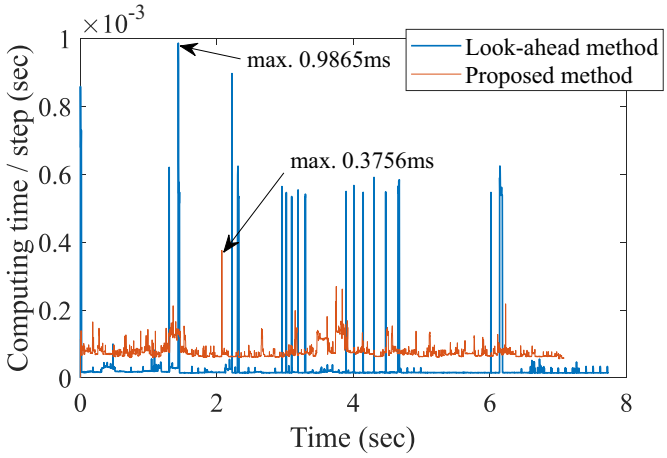

Fig. 17. Comparison of the model computing time in each interpolation step.

As discussed in Section 1, most existing five-axis dual-spline interpolation methods require iterative computation or pre-discretization-based look-ahead processing. The methods needing iterative computation can hardly be applied in real time obviously, while the methods with real-time looking ahead can realize totally online interpolation. For the proposed method, iteration is not required, which means that the advantage is obvious when comparing with existing methods that require iterative computation. However, the advantages and disadvantages of the proposed method comparing with existing looking-ahead-based real-time interpolation methods are not fully clear. Therefore, this section takes a real-time method based on look-ahead window and interval adaptive feedrate scheduling which is recently published [24] for comparison tests.

Aiming at real engineering application, a blade-shape dual-spline toolpath shown in Fig. 13 is employed for the comparison tests. Note that the Z-direction distance between the tooltip spline and the tool-axis spline keeps constant, which means that the perpendicular distance between two splines is non-isometric. The testing parameters are tuned to those shown in Table 2, so as to verify the suitability.

By setting the interpolation period as 0.002 s which is commonly used in industrial machine tools, the obtained tooltip feedrate profiles by the look-ahead window-based method and the proposed method are compared in Fig. 14. In order to avoid using iteration thus achieving the real-time capability, the look-ahead method schedules the feedrate interval by interval, therefore, the zigzag feedrate profile is generated since there exists acceleration/deceleration between two adjacent intervals. Obviously, this is negative to not only the feed motion smoothness and the surface quality, but also the motion efficiency. For the proposed method, above zigzag phenomenon can be solved because the feedrate is obtained by overall filtering but not generated interval by interval. Additionally, the motion time of the toolpath generated by the look-ahead method is 7.742 s, while that of the toolpath generated by the proposed method is 7.082 s. The motion time is reduced by 8.5%. In addition, the FITCE and FIOCE of the proposed method are illustrated in Fig. 15, where it is seen that the errors can be effectively constrained. Translational and rotary axes kinematics parameters are compared in Fig. 16. It can be seen from Fig. 16 that all the parameters can be effectively constrained by the two methods and they perform nearly the same in general, but in detail, the proposed method results in lower fluctuations which is benefit to the motion smoothness. The computation time in each interpolation period for the two methods is shown in Fig. 17. It can be seen from Fig. 17 that although the mean computation

time of the look-ahead-window-based method is relatively low, when the look-ahead processes are executed, they consume large computation burden, while for the proposed FIR-filtering and pseudo-curvature-based method, although the mean computation time is a little longer, the maximum time for step computing is shorter in a large extent. The maximum computation time of the look-ahead method is 0.9865 ms, and that of the proposed method is 0.3756 ms, which decreases by 61.9%. This verifies the advantage of the proposed method in high real-time capability.

To sum up, the proposed five-axis dual-spline interpolation algorithm do not require iterative computation or repetitive discretization, which releases its computation burden and makes it can be realized in real time, and when comparing with existing real-time methods, the proposed one performs better in both motion efficiency and smoothness, as well as in computation time.

4. Conclusion

This paper presents a dual-spline interpolation method for five-axis CNC machine tools. The method is suitable for non-isometric dual spline toolpaths, additionally, neither the iterative computation nor the repetitive discretization of the toolpaths is required, which makes it capable for real-time application. These advantages are realized by the employment of the pseudo curves features and the FIR filtering. First, a translational-axis pseudo curve and a rotary-axis pseudo curve are employed to reduce the dimension of the five-axis dual-spline feedrate-scheduling problem. Second, the relationship between the allowable tooltip feedrate and the geometric features of the pseudo curves under axis drive constraints is established, and this makes it possible to schedule the tooltip feedrate using pseudo curves information instead of original dual-spline information. After that, the scheduled tooltip feedrate is used for generation of five axes velocities, and these axes velocities are filtered by two cascaded FIR filters thus obtaining jerk-bounded feed motions. The filtering releases the requirement of considering the geometric information of adjacent regions when scheduling current tooltip feedrate, which decouples the problem and makes the algorithm free from iteration. Although the filtering will induce errors for the interpolation paths, i.e., the FITCE and FIOCE defined in this paper, they are modeled and constrained by adding two constrain items to the scheduled tooltip feedrate. The filtered axes velocities are integrated so that the axes reference positions, i.e., the output of the five-axis interpolator, can be easily obtained. Illustration and comparison tests are conducted to evaluate the performance of the presented method. It can be seen from the results that the presented method performs well for a typical S-shape dual-spline toolpath which is often utilized for testing the five-axis machine-tool performances and an engineering-derived blade-shape toolpath, and comparing with existing real-time method based on looking ahead, it performs better in motion efficiency and smoothness. In future studies, the proposed method will be used for the global smoothing of five-axis short-line-segment toolpaths.

Declaration of competing interest

The authors declare that they have no known competing financial interests or personal relationships that could have appeared to influence the work reported in this paper.

Acknowledgement

This research is supported by the National Nature Science Foundation of China (52005121), the Nature Science Foundation of Heilongjiang Province (LH2021E034), the China Postdoctoral Science Foundation (2020M681076), the Postdoctoral Science Foundation of Heilongjiang Province (LBH-Z20048), and the Fundamental Research Funds for the Central Universities (3072021CF0705).

References

[1] Yang J, Altintas Y. Generalized kinematics of five-axis serial machines with non-singular tool path generation. Int J Mach Tools Manuf 2013;75:119–32.
[2] Wang L, Yuan X, Si H, Duan F. Feedrate scheduling method for constant peak cutting force in five-axis flank milling process. Chin J Aeronaut 2020;33:2055–69.
[3] Chen Y, Li L. Smooth geodesic interpolation for five-Axis machine tools. IEEE/ASME Trans Mechatron 2016;21:1592–603.
[4] Xu B, Ding Y, Ji W. An interpolation method based on adaptive smooth feedrate scheduling and parameter increment compensation for NURBS curve. ISA Trans 2021. https://doi.org/10.1016/j.isatra.2021.12.003. In press.
[5] Gao X, Zhang S, Qiu L, Liu X, Wang Z, Wang Y. Double B-spline curve-fitting and synchronization-integrated feedrate scheduling method for five-Axis linear-segment toolpath. Appl Sci 2020;10.
[6] Li D, Zhang W, Zhou W, Shang T, Fleischer J. Dual NURBS path smoothing for 5-Axis linear path of flank milling. Int J Precis Eng Manuf 2018;19:1811–20.
[7] Ma J-W, Jia Z-Y, Qin F-Z, Song D-N, Jiang W-W, Chen S-Y. A five-Axis dual NURBS interpolator with constant speed at feedrate-sensitive regions under axial drive constraints. J Manuf Sci Eng 2019;141.
[8] Liu H, Liu Q, Sun P, Liu Q, Yuan S. The optimal feedrate planning on five-axis parametric tool path with geometric and kinematic constraints for CNC machine tools. Int J Prod Res 2016;55:3715–31.
[9] Yang J, Aslan D, Altintas Y. A feedrate scheduling algorithm to constrain tool tip position and tool orientation errors of five-axis CNC machining under cutting load disturbances. CIRP J Manuf Sci Technol 2018;23:78–90.
[10] Dong J, Ferreira PM, Stori JA. Feed-rate optimization with jerk constraints for generating minimum-time trajectories. Int J Mach Tools Manuf 2007;47:1941–55.
[11] Debrouwere F, Van Loock W, Pipeleers G, Dinh QT, Diehl M, De Schutter J, Swevers J. Time-optimal path following for robots with convex-concave constraints using sequential convex programming. IEEE Trans Robot 2013;29:1485–95.
[12] Erkorkmaz K, Chen Q-G, Zhao M-Y, Beudaert X, Gao X-S. Linear programming and windowing based feedrate optimization for spline toolpaths. CIRP Ann 2017;66:393–6.
[13] Sun Y, Chen M, Jia J, Lee Y-S, Guo D. Jerk-limited feedrate scheduling and optimization for five-axis machining using new piecewise linear programming approach. Sci China Technol Sci 2019;62:1067–81.
[14] Lu L, Zhang J, Fuh JYH, Han J, Wang H. Time-optimal tool motion planning with tool-tip kinematic constraints for robotic machining of sculptured surfaces. Robot Cim-Int Manuf 2020;65.
[15] Sang Y, Yao C, Lv Y, He G. An improved feedrate scheduling method for NURBS interpolation in five-axis machining. Precis Eng 2020;64:70–90.
[16] Sencer B, Altintas Y, Croft E. Feed optimization for five-axis CNC machine tools with drive constraints. Int J Mach Tools Manu 2008;48:733–45.
[17] Beudaert X, Lavernhe S, Tournier C. Feedrate interpolation with axis jerk constraints on 5-axis NURBS and G1 tool path. Int J Mach Tools Manuf 2012;57:73–82.
[18] Sun Y, Zhao Y, Bao Y, Guo D. A novel adaptive-feedrate interpolation method for NURBS tool path with drive constraints. Int J Mach Tools Manuf 2014;77:74–81.
[19] Sun YW, Zhao Y, Bao YR, Gu DM. A smooth curve evolution approach to the feedrate planning on five-axis toolpath with geometric and kinematic constraints. Int J Mach Tools Manu 2015;97:86–97.
[20] Liang F, Zhao J, Ji S. An iterative feed rate scheduling method with confined high-order constraints in parametric interpolation. Int J Adv Manuf Technol 2017;92:2001–15.
[21] Liang F, Yan G, Fang F. Global time-optimal B-spline feedrate scheduling for a two-turret multi-axis NC machine tool based on optimization with genetic algorithm. Robot Cim-Int Manuf 2022;75:102308.
[22] Song DN, Ma JW. Interval partition-based feedrate scheduling with axial drive constraints for five-axis spline toolpaths. Int J Adv Manuf Technol 2019;105:4701–14.
[23] Li H, Wang W, Li Q, Huang P. A novel minimum-time feedrate schedule method for five-axis sculpture surface machining with kinematic and geometric constraints. Proc Inst Mech Eng B J Eng Manuf 2018;233:1483–99.
[24] Song D-N, Zhong Y-G, Ma J-W. Look-ahead-window-based interval adaptive feedrate scheduling for long five-axis spline toolpaths under axial drive constraints. Proc Inst Mech Eng B J Eng Manuf 2020;234:1656–70.
[25] Zhang J, Zhang L, Zhang K, Mao J. Double NURBS trajectory generation and synchronous interpolation for five-axis machining based on dual quaternion algorithm. Int J Adv Manuf Technol 2015;83:2015–25.
[26] Qiao Z, Wang T, Wang Y, Hu M, Liu Q. Bézier polygons for the linearization of dual NURBS curve in five-axis sculptured surface machining. Int J Mach Tools Manuf 2012;53:107–17.
[27] Tajima S, Sencer B, Shamoto E. Accurate interpolation of machining tool-paths based on FIR filtering. Precis Eng 2018;52:332–44.
[28] Hayasaka T, Minoura K, Ishizaki K, Shamoto E, Sencer B. A lightweight interpolation algorithm for short-segmented machining tool paths to realize

vibration avoidance, high accuracy, and short machining time. Precis Eng 2019;59:1–17.
[29] Song D-N, Ma J-W, Zhong Y-G, Xiao D, Yao J-J, Zhou C. A fully real-time spline interpolation algorithm with axial jerk constraint based on FIR filtering. Int J Adv Manuf Technol 2021;113:1873–86.
[30] Song D-N, Ma J-W, Zhong Y-G, Yao J-J. Global smoothing of short line segment toolpaths by control-point-assigning-based geometric smoothing and FIR filtering-based motion smoothing. Mech Syst Signal Process 2021;160:107908.
[31] Liu Y, Wan M, Qin X-B, Xiao Q-B, Zhang W-H. FIR filter-based continuous interpolation of G01 commands with bounded axial and tangential kinematics in industrial five-axis machine tools. Int J Mech Sci 2020;169:105325.
[32] Tajima S, Sencer B. Accurate real-time interpolation of 5-axis tool-paths with local corner smoothing. Int J Mach Tools Manu 2019;142:1–15.
[33] Jia ZY, Song DN, Ma JW, Hu GQ, Su WW. A NURBS interpolator with constant speed at feedrate-sensitive regions under drive and contour-error constraints. Int J Mach Tools Manu 2017;116:1–17.